NDⓊ

REPORT DOCUMENTATION PAGE

Form Approved
OMB No. 0704-0188

1. REPORT DATE (DD-MM-YYYY) 18-04-2007	2. REPORT TYPE (Final) Technical Report	3. DATES COVERED (From - To) May 1, 2006 – Sept.30, 2006

4. TITLE AND SUBTITLE

On-Orbit Identification of Inertia Properties of Spacecraft using Robotics Technology

5a. CONTRACT NUMBER
FA9550-06-1-0284

5b. GRANT NUMBER
FA9550-06-1-0284

5c. PROGRAM ELEMENT NUMBER

6. AUTHOR(S)

Ou Ma

5d. PROJECT NUMBER

5e. TASK NUMBER

5f. WORK UNIT NUMBER

7. PERFORMING ORGANIZATION NAME(S) AND ADDRESS(ES)

Regents of New Mexico State
University

P.O. Box 30001, MSC EGR
Las Cruces, NM 88003

8. PERFORMING ORGANIZATION REPORT NUMBER

9. SPONSORING / MONITORING AGENCY NAME(S) AND ADDRESS(ES)

AFOSR – AFRL/VSSV
875 N. Randolph St
Arlington VA 22203
Dr Scott Wells /KM

10. SPONSOR/MONITOR'S ACRONYM(S)

11. SPONSOR/MONITOR'S REPORT NUMBER(S)

12. DISTRIBUTION / AVAILABILITY STATEMENT

Approved for public release. Distribution is unlimited

AFRL-SR-AR-TR-07-0134

13. SUPPLEMENTARY NOTES

14. ABSTRACT

This technical report describes the results of a 6-month research project conducted by Dr. Ou Ma and one of his graduate students at the New Mexico State University under the AFOSR grant # FA9550-06-1-0284 starting in May 2006. In the project, a methodology of on-orbit identification of spacecraft inertia properties (i.e., the mass, the location of the mass center, and the inertia tensor) using a robotic arm was investigated. The extension of the method to using a solar array (instead of a robot) was also preliminarily investigated. The investigation was done in theory and by simulation only because of the time and funding limitations. The ultimate goal of this research is to enhance the control and operation of spacecraft for more challenging autonomous on-orbit service missions in the future.

15. SUBJECT TERMS

16. SECURITY CLASSIFICATION OF:			17. LIMITATION OF ABSTRACT	18. NUMBER OF PAGES	19a. NAME OF RESPONSIBLE PERSON Dr. Ou Ma
a. REPORT	b. ABSTRACT	c. THIS PAGE		52	19b. TELEPHONE NUMBER (include area code) 505-646-6534

Standard Form 298 (Rev. 8-98)
Prescribed by ANSI Std. Z39.18

Final Technical Report

On-Orbit Identification of Inertia Properties of Spacecraft using Robotics Technology

Ou Ma
Ph.D. and Associate Professor, Department of Mechanical Engineering
New Mexico State University, Las Cruces, New Mexico 88005

Hung Dan
Ph.D. student, Department of Electrical and Computer Engineering
New Mexico State University, Las Cruces, New Mexico 88005

December 2006

20070426205

1

Summary

This technical report describes the results of a 6-month research project conducted by Dr. Ou Ma and one of his graduate students at the New Mexico State University under the AFRL/AFOSR grant # FA9550-06-1-0284 starting in summer of 2006. In the project, a methodology of on-orbit identification of spacecraft inertia properties (i.e., the mass, the location of the mass center, and the inertia tensor) using a robotic arm was investigated. The extension of the method to using a solar array (instead of a robot) was also preliminarily investigated. The investigation was done in theory and by simulation only because of the time and funding limitations. The ultimate goal of this research is to enhance the control and operation of spacecraft for more challenging autonomous on-orbit service missions in the future.

The investigated method makes use of an onboard robotic arm to change the inertia distribution of the spacecraft system. As the result of the inertia redistribution, the velocity of the spacecraft system will change correspondingly. Since the velocity change is measurable and the inertia change of the robotic arm is precisely computable, the inertia parameters of the spacecraft body become the only unknown in the momentum equations and hence, can be identified. To treat the problem as a linear identification problem (easier to handle and solve), the problem has to be formulated in two steps (or two sub-problems). The first step is to identify the mass and mass center of the spacecraft; and the second step is to identify the inertia tensor of the spacecraft. The largest advantages of this method are: 1) it does not consume fuel because an onboard mechanical subsystem is energized by solar power; 2) it requires to measure steady-state velocities only (requiring no acceleration and force measurements) because it is based on the momentum conservation law; 3) it will not be affected by any internal energy dissipation, which is very difficult to predict otherwise. On the contrary, the existing thrust force based inertia identification methods will not have these desirable advantages.

Most of the research results reported in this document has been orally presented to and discussed with the Dynamics and Control Group of AFRL/VSSV at Kirtland Air Force Base on September 27, 2006.

Acknowledgement

TABLE OF CONTENTS

1. INTRODUCTION

1,1 Goals and Objectives

This research is aimed at developing a new method for on-orbit identifying inertia properties of spacecraft. The ultimate goal is to enhance the control and operation of spacecraft for more challenging autonomous on-orbit service missions in the future.

This document summarizes the results of a short-term research project conducted by the authors of the document at NMSU in the summer and fall of 2006. The objectives of the project were:

a) Develop a method of using an onboard robotic arm (or arms) to identify the inertia parameters of spacecraft. Conduct a thorough literature survey about the related techniques.

b) Perform a theoretical study of the method in fundamental aspects such as robustness, accuracy, efficiency, or any other potential issues. Develop corresponding solution techniques should issues/difficulties be discovered.

c) Implement a simulation model on ADAMS and data analysis program on Matlab to support the research. The simulation model should include a rigid spacecraft, a 6-DOF rigid-body robotic arm, and sensor models.

d) Explore the possibilities of following the same idea but using other means for inertia identification. For example, use solar arrays, antennas, other re-configurable mechanisms, or fuel level, as opposed to use a robotic arm.

e) Proposed a concept of experimental verification of the proposed method in the lab and on orbit. The concept should be based on the available lab infrastructure at either NMSU or AFRL.

These objectives will help AFRL understand the proposed new method and its potential benefits and limitations with respect to the Air Force missions in space.

1.2 Background and Application

Spacecraft inertia parameters can change in orbit for many reasons such as fuel consumption, hardware reconfiguration, payload deployment, capturing of a flyer, docking with a satellite, or some mechanical malfunctions like an unexpected deployment failure. Spacecraft state-estimator or control system needs to know the correct inertia parameters. For example, after a servicing spacecraft docked to a target satellite for servicing, the active vehicle has to stabilize the compound two-vehicle system before a service job can be performed. Such a stabilization operation cannot be done optimally (in the sense of fuel economy, time efficiency, dynamic impact, etc.) if the active vehicle does not have knowledge of the new inertia properties of the compound system.

Robotics-based (unmanned) satellite on-orbit servicing has been gaining increasing attention in the international space community. Several technology development and demonstration missions have been either done recently or planned in the near future around the world [1-6]. There are significant advantages for having a robotics-based mission to rescue or service a satellite in space for economical or emergency purposes. However, enabling technologies required for autonomous on-orbit servicing have not been all mature. Many research activities are still going on around the world currently. Japan completed an on-orbit technology demonstration mission ETS-7 in 1999 [1]. In that mission, docking and simple robotic operations were tested under the condition that all details of spacecraft are perfectly known. DARPA and USAF is currently developing a technology demonstration mission through the Orbital Express Program [2]. In that mission, more advanced robotics and docking operations including capturing and refuelling

4

will be exercised on orbit. However, the servicing spacecraft still perfectly knows the serviced satellite and the relative motion between the two spacecraft is still gentle. Germany and Canada are also jointly developing a spacecraft rescue-and-service mission called TECSAS [4-5]. In that mission, the rescuing spacecraft will be launched two years after the target satellite, which will also have a slight tumbling motion during the capture operation. In that case, identification of target satellite's inertia properties may become desirable. Future on-orbit rescue and service missions will face more aggressive scenarios such as to capture a tumbling satellite with unknown inertia. In such a mission, quick identification of the inertia properties of the target satellite or the post-capture compound system will be the key for the capture and post-capture operations.

All of the existing techniques for on-orbit identification of inertia parameters rely on an active attitude control system using either thrusters or momentum wheels to perform identification manoeuvres. In this research a robotics-based method is proposed and investigated. The method uses a robotic arm, which is usually available on servicing spacecraft, to help identify the inertia properties. Taking advantage of the well developed robotics technology, the method offers several benefits over the existing methods, as described in Section 2.8. The largest advantage of using a robotic arm to do the inertia identification is that it requires no fuel consumption because an onboard robot is energized by solar power as opposed to fuel. The method can also be extended to using solar arrays or other motion-controllable onboard mechanisms (instead of a robot) to identify inertia properties of spacecraft.

1.3 Literature Survey

There exist several methods for on-orbit identification of inertia properties [7-13]. Although they are different in details, most of them (i.e., [7-12]) use the same fundamental approach, which is based on the Newton-Euler equation of motion, namely,

$$m_s \dot{\mathbf{v}} - m_s [\boldsymbol{\rho}_s \times \dot{\boldsymbol{\omega}} + (\boldsymbol{\rho}_s \times \boldsymbol{\omega}) \times \boldsymbol{\omega}] = \Sigma \mathbf{f}_i \tag{1}$$

$$\mathbf{I}_s \dot{\boldsymbol{\omega}} + \boldsymbol{\omega} \times \mathbf{I}_s \boldsymbol{\omega} + m_s \boldsymbol{\rho}_s \times \dot{\mathbf{v}} = \Sigma \boldsymbol{\tau} + \Sigma(\boldsymbol{\rho}_i \times \mathbf{f}_i) \tag{2}$$

where scalar m_s, vector $\boldsymbol{\rho}_s$ and matrix $\mathbf{I}_s$ are the mass, position vector of mass center, and inertia matrix of the spacecraft with respect to the spacecraft frame, respectively. These three terms are exactly the inertia properties to be identified. Other terms in eqs.(1) and (2) are: $\dot{\mathbf{v}}$ being the acceleration vector of the origin of the spacecraft frame; $\boldsymbol{\omega}$ and $\dot{\boldsymbol{\omega}}$ being the angular velocity and acceleration vectors of the spacecraft which have to be measured; $\Sigma \boldsymbol{\rho}_i \times \mathbf{f}_i$ being the resultant torque of the individual thrust forces $\mathbf{f}_i$; and $\Sigma \boldsymbol{\tau}$ being the resultant moment from other external sources such as gravity-gradient, residual air drag, and solar pressure. In order to estimate the unknown inertia properties from equations (1) and (2), one can convert the two equations into a regression form and then applies the least-square or other filtering techniques to solve it for the unknown components of m_s, $\boldsymbol{\rho}_s$ and $\mathbf{I}_s$ (or $\mathbf{I}_s^{-1}$ instead). It is easy to understand from the two equations that such an approach requires measuring not only the velocities but also the accelerations and the fired thrust forces of the spacecraft. The procedure can be roughly illustrated in Fig.1

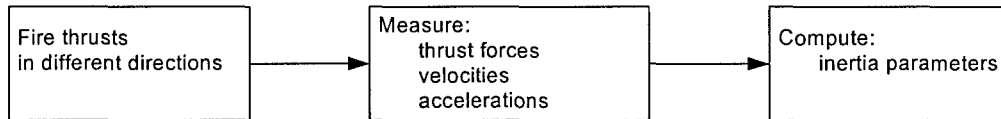| Fire thrusts in different directions	→	Measure: thrust forces velocities accelerations	→	Compute: inertia parameters

Fig.1 Procedure of force-based approach for on-orbit identification of inertia properties

Precisely measuring the time history of the magnitude and direction of each thrust force is difficult. References [7-10] basically followed the above outlined approach. References [11] and [12] smartly

improved the above-mentioned force-based approach by eliminating the nonlinear term $\boldsymbol{\omega} \times \mathbf{I}\boldsymbol{\omega}$ from the regression equation by pre-multiplying $\boldsymbol{\omega} \times$ to each term of eq.(2). This means that, instead of using the vector equation, a specific projection perpendicular to $\boldsymbol{\omega}$ is used to form the regression system for identification. This improves the estimation process but the method still requires known external excitations (such as firing thrusts). Without external excitations, the method works only for rotating spacecraft with an assumption that the initial rotational kinetic energy is already known. The work reported in [12] also considered the effect of the gravity-gradient torques to the identification results.

The only published work which is fundamentally different from the above-mentioned force-based approach is the one reported by [13]. That approach is based on the principle of conservation of angular momentum and thus, is a momentum-based approach. The method uses momentum wheels and the associated attitude control system to perform a set of attitude manoeuvres and then measures the corresponding attitude, angular velocity, and wheel momentum for the identification process. Since the motion (or degrees of freedom) of a momentum wheel is limited and the method is based on angular momentum equation only, it cannot identify the mass and position of mass center of the spacecraft.

Identification of the inertia properties of spacecraft using an onboard robotic arm is a new approach. The closest works published in the literature would be [14-15] where the authors proposed methods of identifying the inertia properties of a payload handled by a robotic arm in space. The references discussed both momentum-based method and force-based methods for identification of the inertia parameters of the robot's payload.

The possibility of identifying spacecraft inertia parameters using solar arrays has never been studied and reported in the open literature. Hence, no survey results in this regard can be reported.

2.   METHODOLOGY

2.1 Basic Concept

This subsection gives a brief idea about the proposed method for those who do not want to go through the full mathematical description of the method. The complete and detailed description is presented in the next few subsections.

The proposed method is based on the principle of impulse and momentum. For easy understanding of the concept, let us first assume no external forces and torques applied to the spacecraft system (which consists of both the spacecraft body and the robotic arm). Because of no impulse from external forces and torques, the angular momentum of the system will be conserved, namely,

$$\mathbf{h}_C = (\mathbf{I}_S + \mathbf{I}_R)\omega = \text{constant vector} \tag{3}$$

where $\mathbf{h}_C$ is the angular momentum of the system; ω is the angular velocity of the system; $\mathbf{I}_S$ and $\mathbf{I}_R$ are the inertia matrices of the spacecraft body and the robotic arm, respectively.
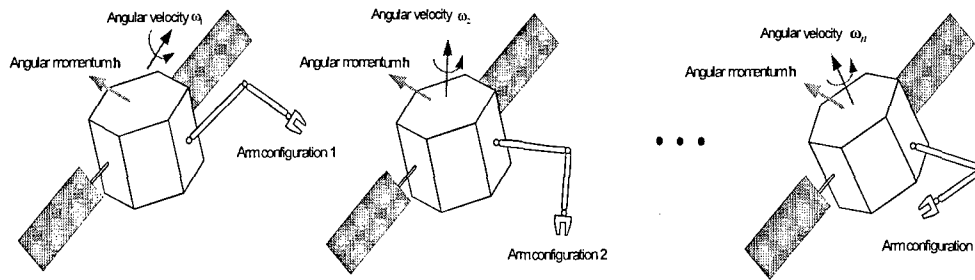

Fig.2 The arm moves to different positions (configurations)

The angular momentum will be conserved even if the robotic arm moves from one configuration to another with respect to the spacecraft body, as shown in Fig.2. In other word, at different arm configurations, we have

$$\mathbf{h}_C = (\mathbf{I}_S + \mathbf{I}_{R1})\omega_1 = (\mathbf{I}_S + \mathbf{I}_{R2})\omega_2 = \cdots = (\mathbf{I}_S + \mathbf{I}_{Rn})\omega_n = \text{constant vector} \tag{4}$$

where $\mathbf{I}_{R1}, \mathbf{I}_{R2}, \cdots, \mathbf{I}_{Rn}$ and $\omega_1, \omega_1, \cdots, \omega_n$ are the inertia matrices of the robotic arm and angular velocities of the system corresponding to the arm configurations 1, 2, ? , n, respectively.

The inertia matrix of the robot at each configuration can be computed using the robot's dynamics model and the known joint positions. The angular velocity of the spacecraft system can be measured using rate sensors. Thus, the only unknown remaining in equation (4) is the inertia matrix of the spacecraft body $\mathbf{I}_S$ and, therefore, it can be solved from the equation.

The method makes use of an onboard robotic arm to excite the dynamics of the spacecraft and then measure the resulting angular velocity changes as input for identification procedure, which can be briefly illustrated in Fig.3.
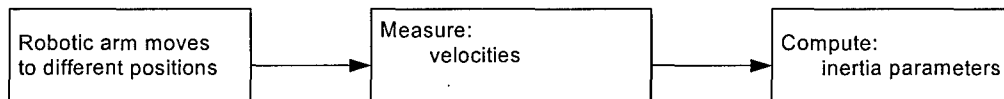

Fig.3 Procedure of the new approach for on-orbit identification of inertia property

7

When external forces and/or torques are not negligible, the resultant impulse generated by the resultant external torque must be added to equation (4). The angular impulse between two measurements can be computed as

$$\Delta \mathbf{h}_C = \int_{t_i}^{t_{i+1}} \left[\Sigma \boldsymbol{\tau} + \Sigma (\boldsymbol{\rho}_i \times \mathbf{f}_i) \right] dt \qquad (5)$$

where t_i and t_{i+1} are respectively the times when the ith and $(i+1)$th measurements were taken place.

2.2 Definitions

To facilitate the development and discussion of the formulation, we define some basic terminologies and coordinate systems as follows (referring to Figs. 4 and 5):

Robot or *robotic arm*: the physical arm staring from the shoulder joint to the end-effector (i.e., the tip).

Spacecraft or *Spacecraft body*: the physical spacecraft excluding the robotic arm.

Spacecraft system: the entire spacecraft system including both the spacecraft body and the robotic arm.

C_S: mass center of the spacecraft body.

C_R: mass center of the robotic arm.

C: mass center of the spacecraft system which is also used as the origin of the orbital frame.

O_S: origin of the spacecraft frame which is a fixed point on the spacecraft body.

F_0: inertial frame.

F_E: Earth frame which is an inertial frame originated at the center O_E of the earth.

F_S: spacecraft frame which is fixed to the spacecraft body and originated at point O_S of the spacecraft body.

m_S: mass of the spacecraft body.

m_R: mass of the robotic arm.

$\mathbf{I}_S$: inertia matrix of the spacecraft body with respect to its own mass center C_S. It is a 3□3 constant matrix in the spacecraft body frame.

$\mathbf{I}_R$: inertia matrix of the robotic arm with respect to its own mass center C_R. It is a function of the configuration of the robot with respect to the spacecraft body.

$\mathbf{I}_{S,C}$: inertia matrix of the spacecraft body with respect to the mass center of the spacecraft system C.

$\mathbf{I}_{R,C}$: inertia matrix of the robot with respect to the mass center of the spacecraft system C.

$\mathbf{I}_C$: inertia matrix of the spacecraft system respect to its the mass center C.

$\boldsymbol{\rho}_S$: position vector of the mass center of the spacecraft body with respect to the origin of the spacecraft frame. It is the vector from O_S to C_S.

$\boldsymbol{\rho}_R$: position vector of the mass center of the robot with respect to the origin of the spacecraft frame. It is the vector from O_S to C_R.

$\boldsymbol{\rho}_C$: position vector of the mass center of the spacecraft system with respect to the origin of the spacecraft frame. It is the vector from O_S to C.

8

$\mathbf{c}_S$: position vector of the mass center of the spacecraft body with respect to the mass center of the spacecraft system. It is the vector from C to C_S.

$\mathbf{c}_R$: position vector of the mass center of the robot with respect to the mass center of the spacecraft system. It is the vector from C to C_S.

$\mathbf{p}_C(0)$ is the initial linear momentum of the spacecraft system;

$\mathbf{h}_C(0)$ is the initial angular momentum of the spacecraft system;

$\mathbf{p}_C$ is the linear momentum of the spacecraft system with respect to the mass center C of the system;

$\mathbf{h}_C$ is the angular momentum of the spacecraft system with respect to the mass center C of the system;

$\dot{\mathbf{c}}_S$: velocity vector of the mass center of the spacecraft body with respect to the orbital frame.

$\dot{\mathbf{c}}_R$: velocity vector of the mass center of the robot with respect to the orbital frame.

$\mathbf{v}_S$ is the linear velocity of the origin O_S of the spacecraft frame F_S.

$\boldsymbol{\omega}_S$ is the angular velocity of the spacecraft body. This is also the angular velocity of the robotic arm when it is locked in a specific configuration.

$\Sigma\boldsymbol{\tau}_i$ is the resultant external torque exerted on the spacecraft system; and

$\Sigma\mathbf{f}_i$ is the resultant external forces exerted on the spacecraft system.
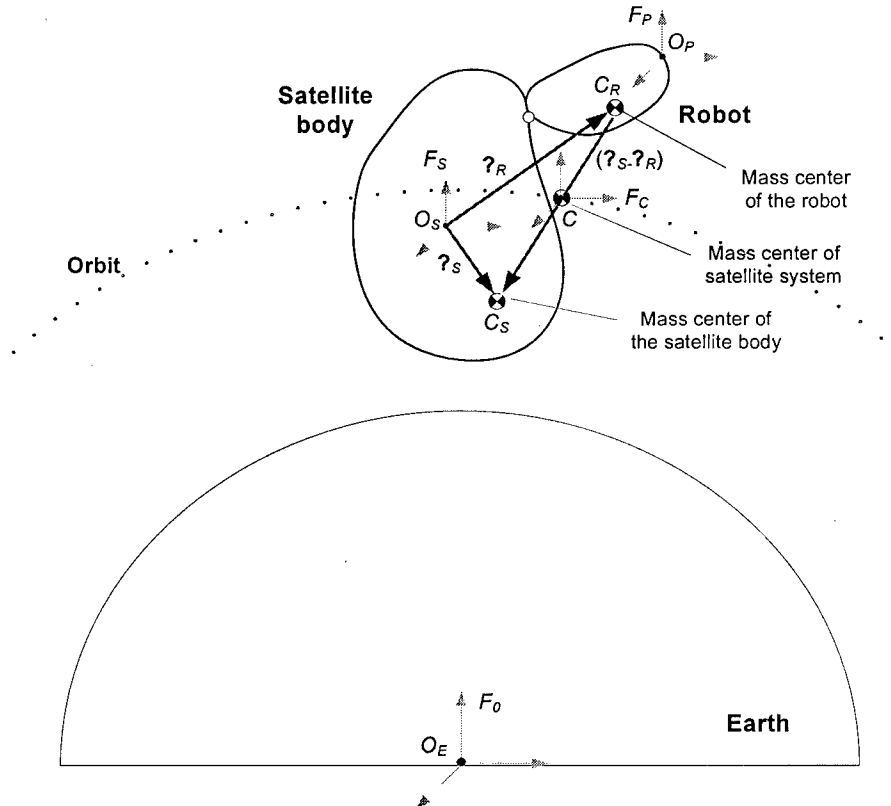

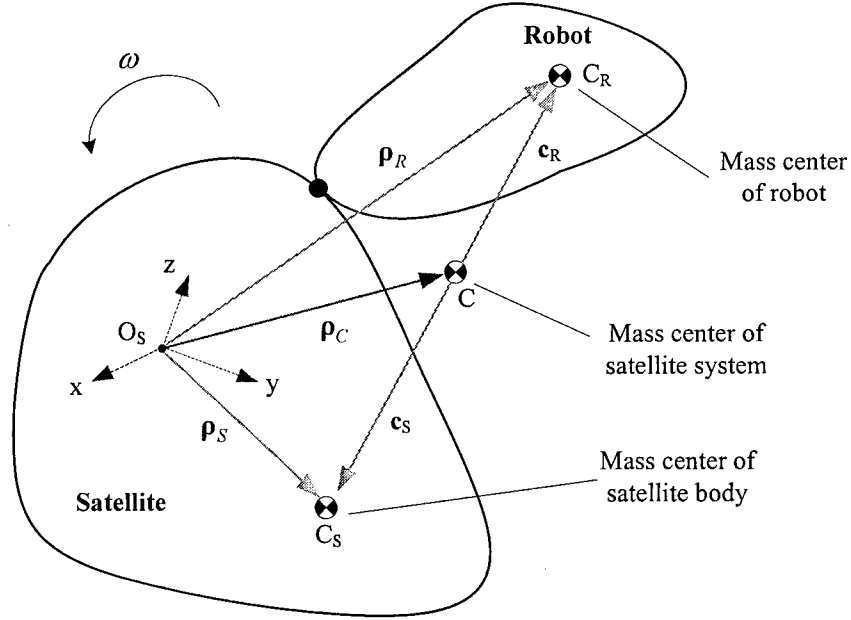Fig.4 Illustration of the coordinate system for dynamics modeling

Fig.5 Mass centers of the robotic arm, the spacecraft body, and the entire spacecraft system

2.3 Basic Kinematics and Dynamics Relations

Based on the definition of mass center and referring to Fig.5, we have the following identities:

$$m_S \mathbf{c}_S + m_R \mathbf{c}_R = \mathbf{0} \quad \text{or} \quad \mathbf{c}_R = -\frac{m_S}{m_R} \mathbf{c}_S$$

$$\boldsymbol{\rho}_C = \frac{m_S \boldsymbol{\rho}_S + m_R \boldsymbol{\rho}_R}{m_S + m_R} \tag{6}$$

from which, we can further derive

$$\mathbf{c}_S = \boldsymbol{\rho}_S - \boldsymbol{\rho}_C = \frac{m_R}{m_S + m_R}(\boldsymbol{\rho}_S - \boldsymbol{\rho}_R)$$

$$\mathbf{c}_R = \boldsymbol{\rho}_R - \boldsymbol{\rho}_C = \frac{m_S}{m_S + m_R}(\boldsymbol{\rho}_R - \boldsymbol{\rho}_S) \tag{7}$$

$$\mathbf{I}_C = \mathbf{I}_S + m_S \left[(\mathbf{c}_S^T \mathbf{c}_S)\mathbf{1} - \mathbf{c}_S \mathbf{c}_S^T \right] + \mathbf{I}_R + m_R \left[(\mathbf{c}_R^T \mathbf{c}_R)\mathbf{1} - \mathbf{c}_R \mathbf{c}_R^T \right]$$

$$= \mathbf{I}_S + \mathbf{I}_R + \frac{m_S m_R}{m_S + m_R} \left((\boldsymbol{\rho}_S - \boldsymbol{\rho}_R)^T (\boldsymbol{\rho}_S - \boldsymbol{\rho}_R)\mathbf{1} - (\boldsymbol{\rho}_S - \boldsymbol{\rho}_R)(\boldsymbol{\rho}_S - \boldsymbol{\rho}_R)^T \right)$$

If the robot is locked in a configuration without relative motion with respect to the spacecraft, then

$$\mathbf{v}_C = \mathbf{v}_S + \boldsymbol{\omega}_S \times \boldsymbol{\rho}_C$$

$$\mathbf{v}_{C_S} = \dot{\mathbf{c}}_S = \mathbf{v}_S + \boldsymbol{\omega}_S \times \boldsymbol{\rho}_S \tag{8}$$

$$\mathbf{v}_{C_R} = \dot{\mathbf{c}}_R = \mathbf{v}_S + \boldsymbol{\omega}_S \times \boldsymbol{\rho}_R$$

10

The dynamics equation of the spacecraft system

$$\frac{d\mathbf{h}_C}{dt} = \frac{d(\mathbf{I}_C\boldsymbol{\omega})}{dt} = \Sigma\boldsymbol{\tau} + \Sigma(\boldsymbol{\rho}_i \times \mathbf{f}_i) \tag{9}$$

or in integration form as

$$\mathbf{h}_C = \mathbf{I}_C\boldsymbol{\omega} = \mathbf{h}_C(0) + \int_0[\Sigma\boldsymbol{\tau} + \Sigma(\boldsymbol{\rho}_i \times \mathbf{f}_i)]dt \tag{10}$$

The following is an important identity which has been repeatedly used in the derivation of the formulation:

$$\boldsymbol{\rho} \times (\boldsymbol{\omega} \times \boldsymbol{\rho}) = (\boldsymbol{\rho}^T\boldsymbol{\rho})\boldsymbol{\omega} - (\boldsymbol{\rho}^T\boldsymbol{\omega})\boldsymbol{\rho} = [(\boldsymbol{\rho}^T\boldsymbol{\rho})\mathbf{1} - \boldsymbol{\rho}\boldsymbol{\rho}^T]\boldsymbol{\omega} \tag{11}$$

where $\mathbf{1}$ is the 3×3 identity matrix.

2.4 Method by Measuring both Linear and Angular Velocities

This method is derived based upon the following assumptions:

1) All the external forces and torques exerted on the spacecraft system are ignored.
2) Both linear and angular velocity of the spacecraft body is known (measured or derived from other measured data).
3) The configuration of the robotic arm is known (measured or derived from measured data).
4) Each measurement is done when the robotic arm has locked to a known configuration.

Since no external forces and torques, the linear momentum and angular momentum are conserved, namely

$$\begin{aligned}\mathbf{p}_C &= \mathbf{p}_C(0) \\ \mathbf{h}_C &= \mathbf{h}_C(0)\end{aligned} \tag{12}$$

where $\mathbf{p}_C(0)$ and $\mathbf{h}_C(0)$ are the initial linear and angular momentums of the spacecraft system, respectively. Equation (12) can be expressed in details as

$$\mathbf{p}_C = \mathbf{p}_{S,C} + \mathbf{p}_{R,C} = m_S\dot{\mathbf{c}}_S + m_R\dot{\mathbf{c}}_R = m_S(\mathbf{v}_S + \boldsymbol{\omega}_S \times \boldsymbol{\rho}_S) + m_R(\mathbf{v}_S + \boldsymbol{\omega}_S \times \boldsymbol{\rho}_R) = \mathbf{p}_C(0) \tag{13}$$

$$\begin{aligned}\mathbf{h}_C &= \mathbf{h}_{S,C} + \mathbf{h}_{R,C} = \mathbf{I}_S\boldsymbol{\omega} + \mathbf{c}_S \times m_S\dot{\mathbf{c}}_S + \mathbf{I}_R\boldsymbol{\omega}_S + \mathbf{c}_R \times m_R\dot{\mathbf{c}}_R \\ &= \mathbf{I}_S\boldsymbol{\omega}_S + \mathbf{c}_S \times m_S(\mathbf{v}_S + \boldsymbol{\omega}_S \times \boldsymbol{\rho}_S) + \mathbf{I}_R\boldsymbol{\omega}_S + \mathbf{c}_R \times m_R(\mathbf{v}_S + \boldsymbol{\omega}_S \times \boldsymbol{\rho}_R) \\ &= \mathbf{I}_S\boldsymbol{\omega}_S + \frac{m_Sm_R}{m_S + m_R}(\boldsymbol{\rho}_S - \boldsymbol{\rho}_R) \times (\mathbf{v}_S + \boldsymbol{\omega}_S \times \boldsymbol{\rho}_S) \\ &\quad + \mathbf{I}_R\boldsymbol{\omega}_S - \frac{m_Sm_R}{m_S + m_R}(\boldsymbol{\rho}_S - \boldsymbol{\rho}_R) \times (\mathbf{v}_S + \boldsymbol{\omega}_S \times \boldsymbol{\rho}_R) \\ &= \mathbf{I}_S\boldsymbol{\omega}_S + \mathbf{I}_R\boldsymbol{\omega}_S + \frac{m_Sm_R}{m_S + m_R}(\boldsymbol{\rho}_S - \boldsymbol{\rho}_R) \times [\boldsymbol{\omega}_S \times (\boldsymbol{\rho}_S - \boldsymbol{\rho}_R)] \\ &= \left[\mathbf{I}_S + \mathbf{I}_R + \frac{m_Sm_R}{m_S + m_R}((\boldsymbol{\rho}_S - \boldsymbol{\rho}_R)^T(\boldsymbol{\rho}_S - \boldsymbol{\rho}_R)\mathbf{1} - (\boldsymbol{\rho}_S - \boldsymbol{\rho}_R)(\boldsymbol{\rho}_S - \boldsymbol{\rho}_R)^T)\right]\boldsymbol{\omega}_S \\ &= \mathbf{I}_C\boldsymbol{\omega}_S = \mathbf{h}_C(0)\end{aligned} \tag{14}$$

Note that the unknown inertia variables m_S and $\boldsymbol{\rho}_S$ appear nonlinearly in both equations. This is not suitable for applying linear identification techniques. We can overcome the nonlinear problem by solving the problem in two separate steps. The first step is to identify mass m_S and position vector of mass center and the second step is for the inertia matrix. Details are described next.

Step 1: identification of mass m_S and position of mass center $\boldsymbol{\rho}_S$

Rewrite equation (13) as

$$\frac{m_R}{m_S}\left(\mathbf{v}_S + \boldsymbol{\omega}_S \times \boldsymbol{\rho}_R - \frac{\mathbf{p}_C(0)}{m_R}\right) + \boldsymbol{\omega}_S \times \boldsymbol{\rho}_S = -\mathbf{v}_S \tag{15}$$

which is linear in terms of the unknown terms m_R / m_S and $\boldsymbol{\rho}_S$.

By moving the arm into a sequence of different configurations, $C_1, C_2, \cdots, C_m$, and measuring the resulting linear and angular velocities of the spacecraft body, $(\mathbf{v}_{S1}, \boldsymbol{\omega}_{S1}), (\mathbf{v}_{S1}, \boldsymbol{\omega}_{S1}), \cdots, (\mathbf{v}_{Sm}, \boldsymbol{\omega}_{Sm})$, we can construct a large system of linear regression equations in terms of the unknowns m_R / m_S and $\boldsymbol{\rho}_S$. Then, solve these two unknowns from the linear regression equation using least-square method. Since m_R is a known and constant, we can find m_S easily after have found the unknown term m_R / m_S. We have two options of writing the linear regression equation depending on whether or not the initial linear momentum $\mathbf{p}_C(0)$ is known. The two options will be described next:

Option 1: the initial linear momentum $\mathbf{p}_C(0)$ is known.

If the initial momentum of the system is known, then we can construct the linear regression equations as follows

$$\mathbf{Ax} = \mathbf{b} \tag{16}$$

where

$$\mathbf{x} \equiv \begin{bmatrix} m_R / m_S \\ \boldsymbol{\rho}_S \end{bmatrix}$$

$$\mathbf{A} \equiv \begin{bmatrix} \mathbf{A}_1 \\ \vdots \\ \mathbf{A}_m \end{bmatrix}, \qquad \mathbf{b} \equiv \begin{bmatrix} \mathbf{b}_1 \\ \vdots \\ \mathbf{b}_m \end{bmatrix} \tag{17a}$$

$$\mathbf{A}_k = \begin{bmatrix} \left(\mathbf{v}_{Sk} + \boldsymbol{\omega}_{Sk} \times \boldsymbol{\rho}_{Rk} - \dfrac{\mathbf{p}_C(0)}{m_R}\right) & \boldsymbol{\Omega}_k \end{bmatrix}$$

$$\mathbf{b}_k = -\mathbf{v}_{Sk}$$

$$\boldsymbol{\Omega}_k \equiv \boldsymbol{\omega}_{Sk}{}^{\times} = \begin{bmatrix} 0 & -\omega_{Sk}(3) & \omega_{Sk}(2) \\ \omega_{Sk}(3) & 0 & -\omega_{Sk}(1) \\ -\omega_{Sk}(2) & \omega_{Sk}(1) & 0 \end{bmatrix} \tag{17b}$$

$$k = 1, 2, \cdots, m$$

where $\mathbf{v}_{Sk}$ and $\boldsymbol{\omega}_{Sk}$ are linear and angular velocities of the spacecraft body measured at the kth configuration of the robotic arm. Vector $\boldsymbol{\rho}_{Rk}$ is the position of the mass center of the entire robot when it is at the kth configuration, which can be computed (see Section 2.6).

Option 2: the initial linear momentum $\mathbf{p}_C(0)$ is unknown.

In this case, we need to eliminate the initial momentum. This can be done by re-writing equation (13) as a momentum increment equation as follows

$$\mathbf{p}_C - \mathbf{p}_C(0) = m_S(\Delta\mathbf{v}_{Sk} + \Delta\boldsymbol{\omega}_{Sk} \times \boldsymbol{\rho}_S) + m_R(\Delta\mathbf{v}_{Sk} + \Delta\boldsymbol{\omega}_{Sk} \times \boldsymbol{\rho}_{Rk} + \boldsymbol{\omega}_{S0} \times \Delta\boldsymbol{\rho}_{Rk}) = \mathbf{0} \qquad (18)$$

$\Delta\mathbf{v}_{Sk}$, $\Delta\boldsymbol{\omega}_{Sk}$ and $\Delta\boldsymbol{\rho}_{Rk}$ are the changes of the linear velocity, angular velocity, and mass center of the spacecraft body from the initial configuration to the kth configuration of the robot. $\boldsymbol{\omega}_{S0}$ is the initial angular velocity of the spacecraft. Notice that the resulting equation no longer has the initial momentum term, from which, we can form the following new linear regression equation:

$$\mathbf{A}\mathbf{x} = \mathbf{b} \qquad (19)$$

where

$$\mathbf{x} \equiv \begin{bmatrix} m_R / m_S \\ \boldsymbol{\rho}_S \end{bmatrix}$$

$$\mathbf{A} \equiv \begin{bmatrix} \mathbf{A}_1 \\ \vdots \\ \mathbf{A}_m \end{bmatrix}, \qquad \mathbf{b} \equiv \begin{bmatrix} \mathbf{b}_1 \\ \vdots \\ \mathbf{b}_m \end{bmatrix} \qquad (20a)$$

and

$$\mathbf{A}_k = \begin{bmatrix} (\Delta\mathbf{v}_{Sk} + \Delta\boldsymbol{\omega}_{Sk} \times \boldsymbol{\rho}_{Rk} + \boldsymbol{\omega}_{S0} \times \Delta\boldsymbol{\rho}_{Rk}) & \boldsymbol{\Omega}_k \end{bmatrix}$$

$$\mathbf{b}_k = -\Delta\mathbf{v}_{Sk}$$

$$\boldsymbol{\Omega}_k \equiv \Delta\boldsymbol{\omega}_{Sk}^{\times} = \begin{bmatrix} 0 & -\Delta\omega_{Sk}(3) & \Delta\omega_{Sk}(2) \\ \Delta\omega_{Sk}(3) & 0 & -\Delta\omega_{Sk}(1) \\ -\Delta\omega_{Sk}(2) & \Delta\omega_{Sk}(1) & 0 \end{bmatrix} \qquad (20b)$$

$$\Delta\boldsymbol{\omega}_{Sk} = \boldsymbol{\omega}_{Sk} - \boldsymbol{\omega}_{S0}$$

$$\Delta\boldsymbol{\rho}_{Rk} = \boldsymbol{\rho}_{Rk} - \boldsymbol{\rho}_{R0}$$

$$k = 1, 2, \cdots, m.$$

Note that using the relative velocities $\Delta\mathbf{v}_{Sk}$ and $\Delta\boldsymbol{\omega}_{Sk}$ for identification has two advantages in comparison of using the absolute velocities $\mathbf{v}_{Sk}$ and $\boldsymbol{\omega}_{Sk}$: (1) the relative velocities can be easily obtained from integrating acceleration data; (2) relative velocities have less measurement bias (i.e., systematic errors).

Step 2: identification of inertia matrix $\mathbf{I}_S$

After completion of Step 1, the inertia variables m_S and $\boldsymbol{\rho}_S$ become known. Then we can identify the inertia matrix $\mathbf{I}_S$. Again, these are two options depending on whether the initial angular momentum is known or not.

<u>Option 1</u>: the initial angular momentum $\mathbf{h}_C(0)$ is known

Based on equation (14), we can construct the following linear regression equation:

$$\mathbf{By} = \mathbf{c} \tag{21}$$

where

$$\mathbf{y} \equiv \begin{bmatrix} I_S(1,1) \\ I_S(2,2) \\ I_S(3,3) \\ I_S(1,2) \\ I_S(1,3) \\ I_S(2,3) \end{bmatrix}, \qquad \mathbf{B} \equiv \begin{bmatrix} \mathbf{B}_1 \\ \vdots \\ \mathbf{B}_m \end{bmatrix}, \qquad \mathbf{c} \equiv \begin{bmatrix} \mathbf{c}_1 \\ \vdots \\ \mathbf{c}_m \end{bmatrix} \tag{22a}$$

$$\mathbf{B}_k = \begin{bmatrix} \omega_{Sk}(1) & 0 & 0 & \omega_{Sk}(2) & \omega_{Sk}(3) & 0 \\ 0 & \omega_{Sk}(2) & 0 & \omega_{Sk}(1) & 0 & \omega_{Sk}(3) \\ 0 & 0 & \omega_{Sk}(3) & 0 & \omega_{Sk}(1) & \omega_{Sk}(2) \end{bmatrix}$$

$$\mathbf{c}_k = \mathbf{h}_C(0) - \mathbf{I}_{Rk}\boldsymbol{\omega}_{Sk} - \frac{m_R m_S}{m_S + m_R}(\boldsymbol{\rho}_S - \boldsymbol{\rho}_{Rk}) \times \left[\boldsymbol{\omega}_{Sk} \times (\boldsymbol{\rho}_S - \boldsymbol{\rho}_{Rk})\right] \tag{22b}$$

$$k = 1, 2, \cdots, m.$$

where $\boldsymbol{\omega}_{Sk}$ is the angular velocity of the spacecraft body measured at the kth configuration of the robotic arm. Terms $\boldsymbol{\rho}_{Rk}$ and $\mathbf{I}_{Rk}$ are the position of the mass center and the centroid inertia matrix of the entire robot when it is at the kth configuration, which can be computed from the robot model (see Section 2.6). Term $I_S(i,j)$ is the (i,j)th component of the inertia matrix $\mathbf{I}_S$.

<u>Option 2</u>: the initial angular momentum $\mathbf{h}_C(0)$ is unknown

In this case, we need to eliminate the initial momentum. This can be done by re-writing equation (14) as a momentum increment equation as follows

$$\begin{aligned}
\mathbf{h}_C - \mathbf{h}_C(0) &= \mathbf{I}_S \Delta\boldsymbol{\omega}_{Sk} \\
&+ \left[\mathbf{I}_{Rk} + \frac{m_R m_S}{m_S + m_R}\left((\boldsymbol{\rho}_S - \boldsymbol{\rho}_{Rk})^T(\boldsymbol{\rho}_S - \boldsymbol{\rho}_{Rk})\mathbf{1} - (\boldsymbol{\rho}_S - \boldsymbol{\rho}_{Rk})(\boldsymbol{\rho}_S - \boldsymbol{\rho}_{Rk})^T\right)\right]\Delta\boldsymbol{\omega}_{Sk} \\
&+ \left[\mathbf{I}_{Rk} - \mathbf{I}_{R0} + \frac{m_R m_S}{m_S + m_R}\left((\boldsymbol{\rho}_S - \boldsymbol{\rho}_{Rk})^T(\boldsymbol{\rho}_S - \boldsymbol{\rho}_{Rk})\mathbf{1} - (\boldsymbol{\rho}_S - \boldsymbol{\rho}_{Rk})(\boldsymbol{\rho}_S - \boldsymbol{\rho}_{Rk})^T\right)\right]\boldsymbol{\omega}_{S0} \\
&- \frac{m_R m_S}{m_S + m_R}\left((\boldsymbol{\rho}_S - \boldsymbol{\rho}_{R0})^T(\boldsymbol{\rho}_S - \boldsymbol{\rho}_{R0})\mathbf{1} - (\boldsymbol{\rho}_S - \boldsymbol{\rho}_{R0})(\boldsymbol{\rho}_S - \boldsymbol{\rho}_{R0})^T\right)\boldsymbol{\omega}_{S0} \\
&= 0
\end{aligned} \tag{23}$$

$$k = 1, 2, \cdots, m$$

14

where $\Delta\boldsymbol{\omega}_{Sk} = \boldsymbol{\omega}_{Sk} - \boldsymbol{\omega}_{S0}$ is the increment of the angular velocity of the spacecraft body from the initial configuration to the kth configuration of the robotic arm. Hence, we can form the following new linear regression equation:

$$\mathbf{B}\mathbf{y} = \mathbf{c} \tag{24}$$

where

$$\mathbf{y} \equiv \begin{bmatrix} I_S(1,1) \\ I_S(2,2) \\ I_S(3,3) \\ I_S(1,2) \\ I_S(1,3) \\ I_S(2,3) \end{bmatrix}, \qquad \mathbf{B} \equiv \begin{bmatrix} \mathbf{B}_1 \\ \vdots \\ \mathbf{B}_m \end{bmatrix}, \qquad \mathbf{c} \equiv \begin{bmatrix} \mathbf{c}_1 \\ \vdots \\ \mathbf{c}_m \end{bmatrix} \tag{25a}$$

$$\mathbf{B}_k = \begin{bmatrix} \Delta\omega_{Sk}(1) & 0 & 0 & \Delta\omega_{Sk}(2) & \Delta\omega_{Sk}(3) & 0 \\ 0 & \Delta\omega_{Sk}(2) & 0 & \Delta\omega_{Sk}(1) & 0 & \Delta\omega_{Sk}(3) \\ 0 & 0 & \Delta\omega_{Sk}(3) & 0 & \Delta\omega_{Sk}(1) & \Delta\omega_{Sk}(2) \end{bmatrix}$$

$$\mathbf{c}_k = -\left[\mathbf{I}_{Rk} + \frac{m_R m_S}{m_S + m_R} \mathbf{T}_k \right] \Delta\boldsymbol{\omega}_{Sk} - \left[\mathbf{I}_{Rk} - \mathbf{I}_{R0} + \frac{m_R m_S}{m_S + m_R} (\mathbf{T}_k - \mathbf{T}_0) \right] \boldsymbol{\omega}_{S0}$$

$$\mathbf{T}_k = (\boldsymbol{\rho}_S - \boldsymbol{\rho}_{Rk})^T (\boldsymbol{\rho}_S - \boldsymbol{\rho}_{Rk}) \mathbf{1} - (\boldsymbol{\rho}_S - \boldsymbol{\rho}_{Rk})(\boldsymbol{\rho}_S - \boldsymbol{\rho}_{Rk})^T \tag{25b}$$

$$\mathbf{T}_0 = (\boldsymbol{\rho}_S - \boldsymbol{\rho}_{R0})^T (\boldsymbol{\rho}_S - \boldsymbol{\rho}_{R0}) \mathbf{1} - (\boldsymbol{\rho}_S - \boldsymbol{\rho}_{R0})(\boldsymbol{\rho}_S - \boldsymbol{\rho}_{R0})^T$$

$$k = 1, 2, \cdots, m.$$

2.5 Method by Measuring Angular Velocity Only

The approach introduced in Section 2.4 requires that both the linear and angular velocities of the spacecraft are known. Measurement of the linear velocity is not as easy as the measurement of angular velocity. Usually, linear velocity is integrated from accelerometer data, which will have drifting errors. In this section, we introduce an alternative approach which does not require the known linear velocity of the spacecraft. This method is derived based upon the following assumptions:

1) All the external forces and torques exerted on the spacecraft system are ignored.

2) The angular velocity of the spacecraft body is known (measured or derived from measured data).

3) The configuration of the robotic arm is known (measured or derived from measured data).

4) Each measurement is done when the robotic arm has locked to a known configuration.

Since no external forces and torques, the angular momentum is conserved, namely,

$$\mathbf{I}_C \boldsymbol{\omega}_S = \mathbf{h}_C(0) \tag{26}$$

Notice that the inertia matrix of the spacecraft system is the sum of the inertia matrices of the spacecraft body and the robotic arm, namely,

$$\mathbf{I}_C = \mathbf{I}_{S,C} + \mathbf{I}_{R,C} \tag{27}$$

Based on the definitions of inertia matrix and mass center, we have

15

$$\mathbf{I}_{S,C} = \mathbf{I}_S + m_S \left[(\mathbf{c}_S^T \mathbf{c}_S)\mathbf{1} - \mathbf{c}_S \mathbf{c}_S^T \right]$$

$$= \mathbf{I}_S + m_S \left(\frac{m_R^2}{(m_S + m_R)^2} \right) \left[(\boldsymbol{\rho}_S - \boldsymbol{\rho}_R)^T (\boldsymbol{\rho}_S - \boldsymbol{\rho}_R)\mathbf{1} - (\boldsymbol{\rho}_S - \boldsymbol{\rho}_R)(\boldsymbol{\rho}_S - \boldsymbol{\rho}_R)^T \right]$$

$$\mathbf{I}_{R,C} = \mathbf{I}_R + m_R \left[(\mathbf{c}_R^T \mathbf{c}_R)\mathbf{1} - \mathbf{c}_R \mathbf{c}_R^T \right] \tag{28}$$

$$= \mathbf{I}_R + m_R \left(\frac{m_S^2}{(m_S + m_R)^2} \right) \left[(\boldsymbol{\rho}_S - \boldsymbol{\rho}_R)^T (\boldsymbol{\rho}_S - \boldsymbol{\rho}_R)\mathbf{1} - (\boldsymbol{\rho}_S - \boldsymbol{\rho}_R)(\boldsymbol{\rho}_S - \boldsymbol{\rho}_R)^T \right]$$

where $\mathbf{1}$ is the 3×3 identity matrix. Substituting (27) and (28) into equation (26), we get

$$\mathbf{I}_S \boldsymbol{\omega}_S + \left[\frac{m_S^2 m_R + m_S m_R^2}{(m_S + m_R)^2} \right] \left[(\boldsymbol{\rho}_S - \boldsymbol{\rho}_R)^T (\boldsymbol{\rho}_S - \boldsymbol{\rho}_R)\mathbf{1} - (\boldsymbol{\rho}_S - \boldsymbol{\rho}_R)(\boldsymbol{\rho}_S - \boldsymbol{\rho}_R)^T \right] \boldsymbol{\omega}_S = \mathbf{h}_C(0) - \mathbf{I}_R \boldsymbol{\omega}_S \tag{29}$$

This is the fundamental equation for spacecraft inertia identification. In the equation, mass m_S, mass center $\boldsymbol{\rho}_S$, and inertia matrix $\mathbf{I}_S$ are the unknowns to be identified and all the other variables can be either measured or computed. Notice that the inertia matrix $\mathbf{I}_S$ appears linearly in the equation but the mass m_S does not. In order to apply linear regression techniques, all the unknown variables to be identified must be linear in the regression equations. We can solve this problem by defining a new dimensionless variable λ as

$$\lambda \equiv \frac{m_S^2 m_R + m_S m_R^2}{(m_S + m_R)^2} \tag{30}$$

Apparently, λ is a function of m_S. Since one can always find m_S in terms of λ from (30), we will identify λ instead of m_S. To this end, equation (29) is re-written as

$$\mathbf{I}_S \boldsymbol{\omega}_S + \lambda \boldsymbol{\Lambda} \boldsymbol{\omega}_S = \mathbf{h}_C(0) - \mathbf{I}_R \boldsymbol{\omega}_S \tag{31}$$

where

$$\boldsymbol{\Lambda} \equiv \left[(\boldsymbol{\rho}_S - \boldsymbol{\rho}_R)^T (\boldsymbol{\rho}_S - \boldsymbol{\rho}_R)\mathbf{1} - (\boldsymbol{\rho}_S - \boldsymbol{\rho}_R)(\boldsymbol{\rho}_S - \boldsymbol{\rho}_R)^T \right] \tag{32}$$

Since $\mathbf{I}_S$ is symmetric, it actually has only six unknown components. Thus, we can define a minimum set of unknown variables as follows:

$$\mathbf{x} = \begin{bmatrix} x_1 \\ x_2 \\ \vdots \\ x_{10} \end{bmatrix} \equiv \begin{bmatrix} \lambda \\ \rho_S(1) \\ \rho_S(2) \\ \rho_S(3) \\ I_S(1,1) \\ I_S(2,2) \\ I_S(3,3) \\ I_S(1,2) \\ I_S(1,3) \\ I_S(2,3) \end{bmatrix} \tag{33}$$

16

As seen clearly, equation (31) is a nonlinear equation in terms of the unknown **x**, namely,

$$\varphi(\mathbf{x}, \boldsymbol{\rho}_R) = \mathbf{h}_C(0) - \mathbf{I}_R \boldsymbol{\omega}_S \tag{34}$$
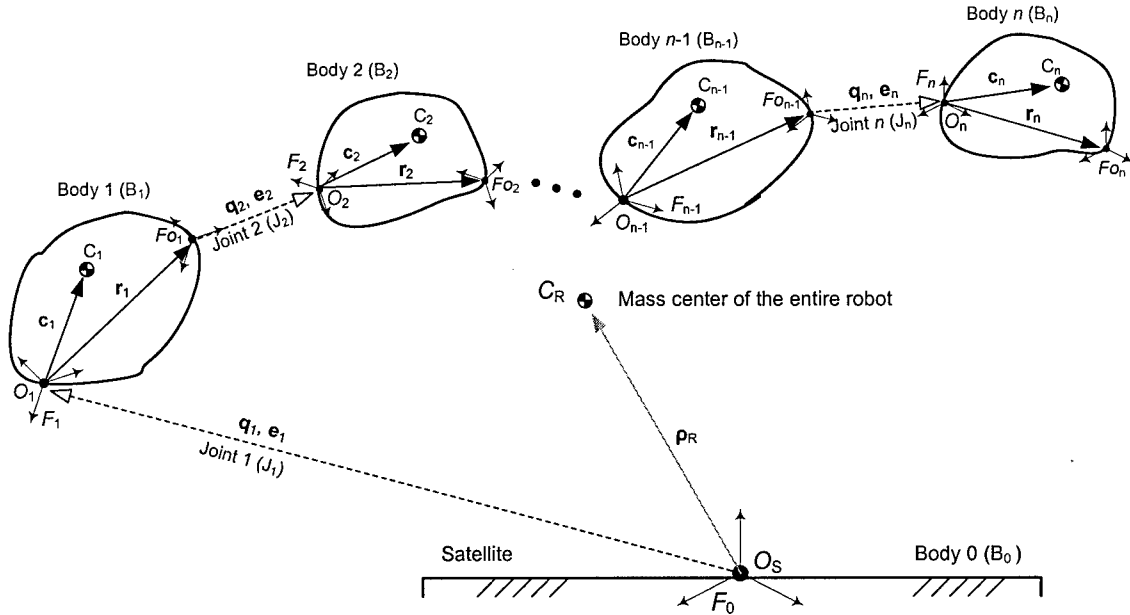
Obviously this is a nonlinear identification problem from which we can solve for **x** in terms of known $\boldsymbol{\rho}_R, \mathbf{I}_R, \mathbf{h}_C(0)$ and $\boldsymbol{\omega}_S$.

2.6 Inertia and Momentum of the Entire Robotic Arm

In this section, we describe the formulation for computing the inertial property (i.e., the mass center and inertia matrix) and momentum of the entire robot. Although the mass center and inertia matrix of the robot will change with the motion of the robot, they can be precisely computed as long as the inertia properties of individual links of the robot are known in advance. This is because the configuration of the robot are fully controlled and known. First, the following assumptions are made:

1) The mass of each body of the robot is constant and known.

2) The position of mass center and inertia matrix of each body of the robot are known. They are constant when they are represented in coordinate frame fixed to their associated body.

3) The configuration and motion of the robot with respect to the spacecraft body are known. This known information can be represented by the joint angles and joint rates of the robot.

The kinematics of the robotic arm is defined as shown in Fig.6.

Notation:

q_i -- Relative displacements (state variable) of Joint i, expressed in Fo_{i-1} frame (the outboard frame of previous body).

e_i -- Relative angular displacements of Joint I (represented by Euler angles or quaternions), expressed in Fo_{i-1}.

r_i -- Intrabody vector of body i, expressed in F_i frame (the inboard frame of the i'th body).

c_i -- Position vector of the center of mass (C_i) of body i with respect to Joint i, expressed in F_i frame.

Fig.6 Kinematics notation of the robotic arm

17

By definition, the position of the mass center and the inertia matrix of the entire robot with respect to the spacecraft frame F_S can be computed as follows:

$$\boldsymbol{\rho}_R = \frac{\sum_{i=1}^{n} m_i \boldsymbol{\rho}_i}{\sum_{i=1}^{n} m_i} \tag{35}$$

$$\mathbf{I}_R = \sum_{i=1}^{n} \mathbf{I}_i \tag{36}$$

where m_i is the mass of the ith link; $\boldsymbol{\rho}_i$ and $\mathbf{I}_i$ are respectively the position vector of the mass center and the inertia matrix of the ith body with respect to the origin of the spacecraft frame F_S and also represented in F_S. They can be computed using the following kinematic relations

$$\mathbf{R}_i = \prod_{k=1}^{i} {}^k \mathbf{R}_k$$

$$\boldsymbol{\rho}_i = \sum_{k=1}^{i} \mathbf{R}_k {}^k r_k + \mathbf{R}_i {}^i \mathbf{c}_i \tag{37}$$

$$\mathbf{I}_i = \mathbf{R}_i {}^i \mathbf{I}_i \mathbf{R}_i^T + m_i \left[(\boldsymbol{\rho}_i^T \boldsymbol{\rho}_i) \mathbf{1} - \boldsymbol{\rho}_i \boldsymbol{\rho}_i^T \right]$$

for $i = 1, 2, \cdots, n$. In the above equations ${}^i\mathbf{c}_i$ and ${}^i\mathbf{I}_i$ are the known mass center and inertia matrix of the ith body with respect to the body fixed frame F_i and, therefore, their values will not change during the robot motion. Moreover, vector ${}^i\mathbf{r}_i$ and matrix ${}^i\mathbf{R}_i$ represent the relative position and orientation from the ith joint (or the ith body frame) to the $(i+1)$th joint or the tip of the arm, expressed in the ith body fixed frame and thus, they are constant too.

Linear and angular momentums of the entire robot, represented in the spacecraft frame, can be computed as follows:

$$\mathbf{l}_R = \sum_{i=1}^{n} m_i \mathbf{v}_{ci} = \sum_{i=1}^{n} m_i \mathbf{v}_{ci}$$

$$\mathbf{h}_R = \sum_{k=1}^{i} \left(\mathbf{I}_i \boldsymbol{\omega}_i + \boldsymbol{\rho}_i \times m_i \mathbf{v}_{ci} \right) \tag{38}$$

where $\mathbf{v}_i$ and $\boldsymbol{\omega}_i$ are the absolute linear and angular velocities of the mass center of the ith link of the robot, which can be computed from the known joint angles and rates using the following recursive formulae:

$$\mathbf{v}_{ci} = \mathbf{v}_{ci-1} + \boldsymbol{\omega}_{i-1} \times \mathbf{R}_{i-1} \left({}^{i-1}\mathbf{r}_{i-1} - {}^{i-1}\mathbf{c}_{i-1} \right) + \boldsymbol{\omega}_i \times \mathbf{R}_i {}^i\mathbf{c}_i$$

$$\boldsymbol{\omega}_i = \boldsymbol{\omega}_{i-1} + \mathbf{R}_i \begin{bmatrix} 0 \\ 0 \\ 1 \end{bmatrix} \dot{\theta}_i \qquad \text{for } i = 1, 2, \cdots, n \tag{39}$$

Note that $\mathbf{v}_0$ and $\boldsymbol{\omega}_0$ are the linear and angular velocities of the spacecraft.

2.7 Technical Issues to be Addressed

18

The above-outlined method is still a concept. In order to prove its feasibility for real space application, it has to be thoroughly studied. At this moment, the following technical challenges have been identified for the proposed research:

1) Since the observability of $\mathbf{I}$ is closely dependent on the mechanical properties and the configurations of the robotic arm, guidelines need to be established as how to select optimal arm poses such that not only all the inertia properties can be identified but also the resulting numerical procedure be robust.

2) Since space robots are usually flexible (for minimizing mass), the effect of arm flexibility onto the identification method needs to be looked into. This may not be a problem because the method requires measuring steady-state $\boldsymbol{\omega}_S$ and $\mathbf{v}_S$ only, so that the measurement can be done after the arm vibration dies down.

3) The effectiveness of the method is related to the ratio of the arm inertia and the spacecraft inertia. If the arm is too light to sufficiently influence the spacecraft, it can hold a piece of spare hardware (with known inertia) from the spacecraft during an identification maneuver.

4) The issue of sensitivity to sensor noise and how to reduce it has to be addressed. This is a common problem for any identification method. Among many available techniques, the most suitable will be identified and tailored to our specific needs.

5) The effect of the gravity-gradient torque on the proposed identification method needs to be investigated. The gravity-gradient torque may be non-negligible if spacecraft is in a LEO orbit. If that is the case, the angular momentum caused by the gravity-gradient must be considered in the formulation.

6) An analysis of computational complexity is required. Since an inertia identification method is usually a part of a spacecraft control system (model-based, adaptive control), it has to be executed at a fast rate with a limited memory space.

In fact, items 3) to 5) are common for any other identification methods too. These problems and any others, which may be unveiled later, will be carefully investigated. Based on the investigation, practical solution measures will be proposed and evaluated.

2.8 Comparison with Other Methods

From a preliminary study of this new method, the following pros and cons are identified:

– Since a robotic arm is energized by solar energy, the method does not consume any fuel of the spacecraft. On the contrary, the propulsion based methods consume fuel.

– The method is based on the conservation-of-momentum principle and thus only velocity data are required. Propulsion based methods require velocity, acceleration, and force data because they are based on equations of motion. Also, force and acceleration data are noisier than velocity data.

– The method requires to measure steady-state velocities only. This will ease and make the measurements much more reliable. Steady-state measurements will have minimal errors caused by the arm dynamics and spacecraft structural dynamics.

– Since the method is based on momentum-conservation, any unknown energy damping in the system will not affect the identification result. On the contrary, any unmodelled damping may corrupt the identification results for a method based on the equations of motion.

– The method identifies the $\mathbf{I}$ matrix directly while the force based methods can only identify $\mathbf{I}^{-1}$ or

$\mathbf{I}$ and $\mathbf{I}^{-1}$ together, which requires additional computations.

- The method requires a robotic arm onboard the spacecraft. However, this will likely be the case for spacecraft designed for servicing a spacecraft on orbit.
- The method requires accurate inertia parameters and kinematics of the robot. These can be guaranteed before launch. After-launch recalibration of robot parameters can be done based on the same (momentum-conservation based) approach before the spacecraft inertia properties have changed.
- As mentioned in [15], the method requires the spacecraft to have an initial angular momentum if the inertia tensor needs to be identified.

3. SIMULATION STUDY

Computer simulation is the only means for the research on this short-term project. In this section the dynamics simulation model and the simulation results are described in details.

3.1 Simulation Model

The dynamics model for the simulation study consists of a rigid spacecraft and a 6-DOF robotic arm. The kinematics of the system, represented by nine coordinate frames, are defined in Figs.7&8. The spacecraft frame F_S is fixed at the geometric center O_S of the spacecraft body. The ith local coordinate frame of the robot is attached to the ith link and originated at the ith joint of the robot ($i = 1, 2, \cdots, 6$). So, the frame will move with the ith link. The tip frame F_7 is attached at the tip of the end-effector, as shown in Figs.7 &8. The home configuration of the robot (where all the joint angles are zero) is shown in Fig.7, namely, the arm being completely folded to the top surface of the spacecraft body. The attaching point of the arm on the spacecraft body is also shown in Fig.8. The kinematics and dynamics parameters of the manipulator implemented in the simulation model are listed in Table 1.

The model has been implemented on ADAMS for dynamic simulation and on Matlab for analysis. The graphics model of the system on ADAMS is shown in Fig.9. Simulation results obtained from the model are presented in the next few subsections along with discussions about the findings.
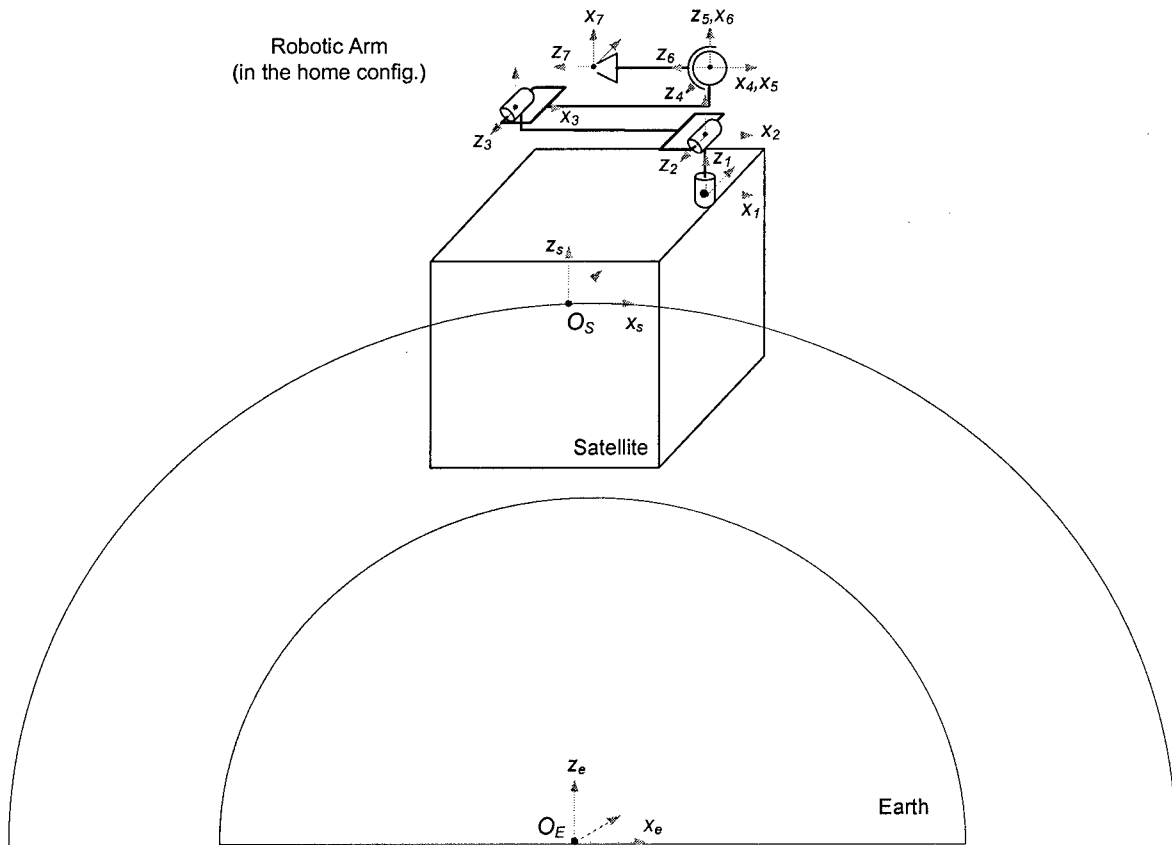

Fig.7 Reference frames of the spacecraft and robotic arm in home configuration
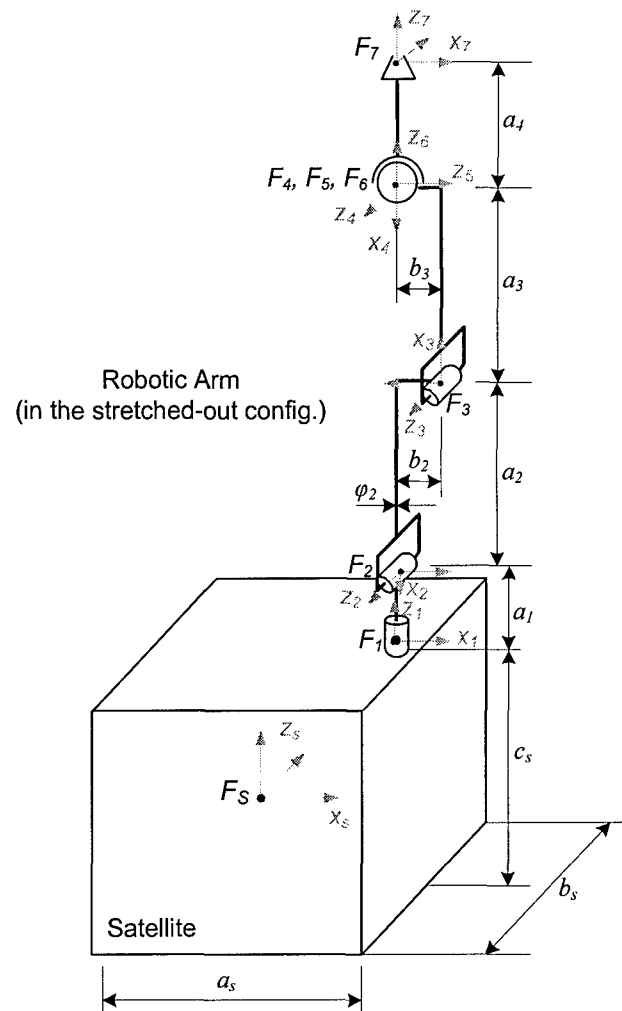
21

Fig.8 Kinematic dimensions of the spacecraft and robotic arm

Table 1 Kinematics and Dynamics Parameters of the Spacecraft-Arm System

Body	Parameters	Unit	Value	Note
Spacecraft	a_s, b_s, c_s	m	1.0, 1.0, 1.0	
	m_S	kg	1000.0	
	$^S\mathbf{c}_S$	m	$\begin{bmatrix} 0 & 0 & 0 \end{bmatrix}^T$	
	$^S\mathbf{I}_S$	kg·m^2	diag(166.67, 166.67, 166.67)	
Link 1	a_1, b_1, ϕ_1	m	0.2, 0.0, 0.025	
	m_1	kg	7.597	
	$^1\mathbf{c}_1$	m	$\begin{bmatrix} 0 & 0 & a_1/2 \end{bmatrix}^T$	

	$^1\mathbf{I}_1$	kg·m²	Computed	
Link 2	a_2, b_2, ϕ_2	m	1.0, 0.2, 0.025	
	m_2	kg	34.885	
	$^2\mathbf{c}_2$	m	$[-a_2/2 \quad b_2/2 \quad 0]^T$	
	$^2\mathbf{I}_2$	kg·m²	Computed	
Link 3	a_3, b_3, ϕ_3	m	1.0, 0.2, 0.025	
	m_3	kg	34.885	
	$^3\mathbf{c}_3$	m	$[a_3/2 \quad b_3/2 \quad 0]^T$	
	$^3\mathbf{I}_3$	kg·m²	Computed	
Link 4 (dummy link)	a_4, b_4, ϕ_4	m	0, 0, 0	
	m_4	kg	0	
	$^4\mathbf{c}_4$	m	$[0 \quad 0 \quad 0]^T$	
	$^4\mathbf{I}_4$	kg·m²	Computed	
Link 5 (dummy link)	a_5, b_5, ϕ_5	m	0, 0, 0	
	m_5	kg	0	
	$^5\mathbf{c}_5$	m	$[0 \quad 0 \quad 0]^T$	
	$^5\mathbf{I}_5$	kg·m²	Computed	
Link 6 (end-effector)	a_6, b_6, ϕ_6	m	0.5, 0.0, 0.025	
	m_6	kg	15.817	
	$^6\mathbf{c}_6$	m	$[0 \quad 0 \quad a_4/2]^T$	
	$^6\mathbf{I}_6$	kg·m²	Computed	

Note that the lengths of the 4th and 5th links are zero because the last three revolute joints are integrated into a 3-DOF spherical joint.
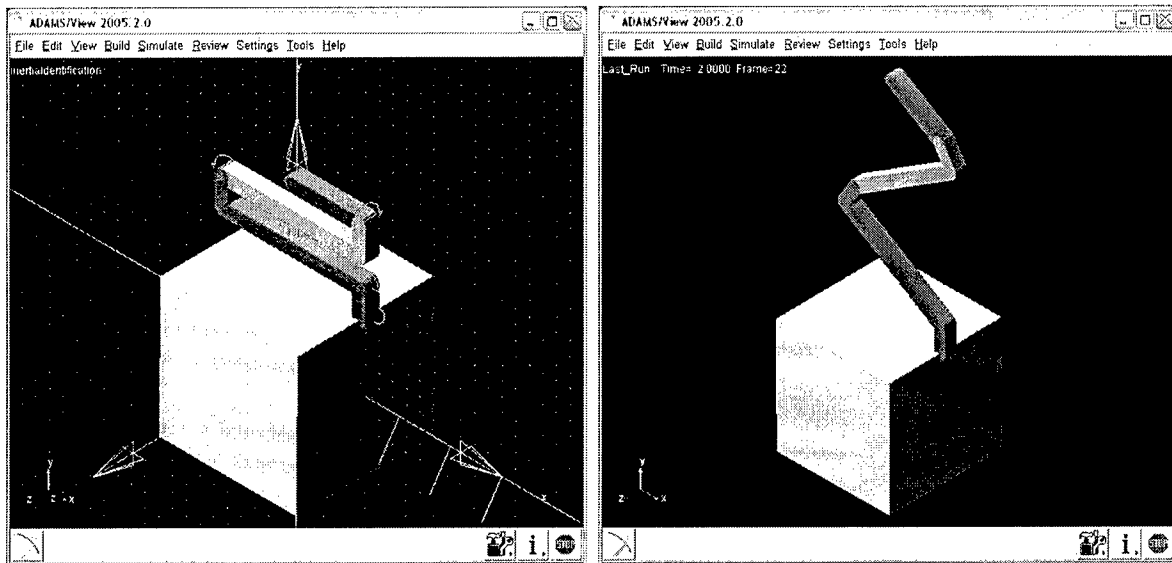
Fig.9 Graphics model of the spacecraft-arm system on ADAMS

3.2 Effect of Arm/Spacecraft Mass Ratio

Since the method is to use a robotic arm to excite the dynamics of the spacecraft so that the inertia properties can be identifiable, it is naturally concerned that the robotic arm has to have sufficiently large inertia in order to be able to excite the dynamics of the spacecraft. To address this concern, a few examples are illustrated in this subsection to see how the identification results vary with respect the ratio between the arm mass and the spacecraft mass.

In theory, the identification result has nothing to do with the arm/spacecraft mass ratio. In other words, the unknown inertia parameters can always be 100% accurately solved from the momentum equations regardless what the mass ratio is as long as the required velocity data are perfect. However, this is not true in practice because the velocity data can never be perfectly accurate. In fact, the effect of the mass ratio is really in the measurement accuracy of the velocity data as opposed to in the identification solution. In general, velocity measurement will have larger relative error when the mass ratio is small because of the correspondingly less signal/noise ratio. This larger error in velocity data will in turn lead to larger identification error. Based on this argument, we will add some errors in the velocity data in order to investigate the effect of arm/spacecraft mass ratio on the performance of the identification method.

In all the examples of this subsection, ten velocity measurements are taken at the configurations equally separated along the path defined in each example. A bias error defined as a percentage of the true velocity value is added to the measured linear velocity or angular velocity (but not both, otherwise the error will be cancelled). The corresponding errors in the identified parameters are computed and plotted.

All the examples show that the identification errors are insensitive to the arm/spacecraft mass ratio as long as the ratio is more than 0.05. This suggests that the mass of the arm does not need to be larger than 5% of the spacecraft's mass in order to get good identification quality.

24

Example 3.2.1:

In this case the arm is commanded to go along the general trajectory A defined in Section 3.3 (see Fig.13). Ten velocity measurements are taken at the configurations equally separated along the path. The spacecraft body is initially spinning about the Z axis at a rate of 5 deg/s. Based on the velocity data, the inertia parameters of the spacecraft are identified. The identification errors are plotted in Fig.10.
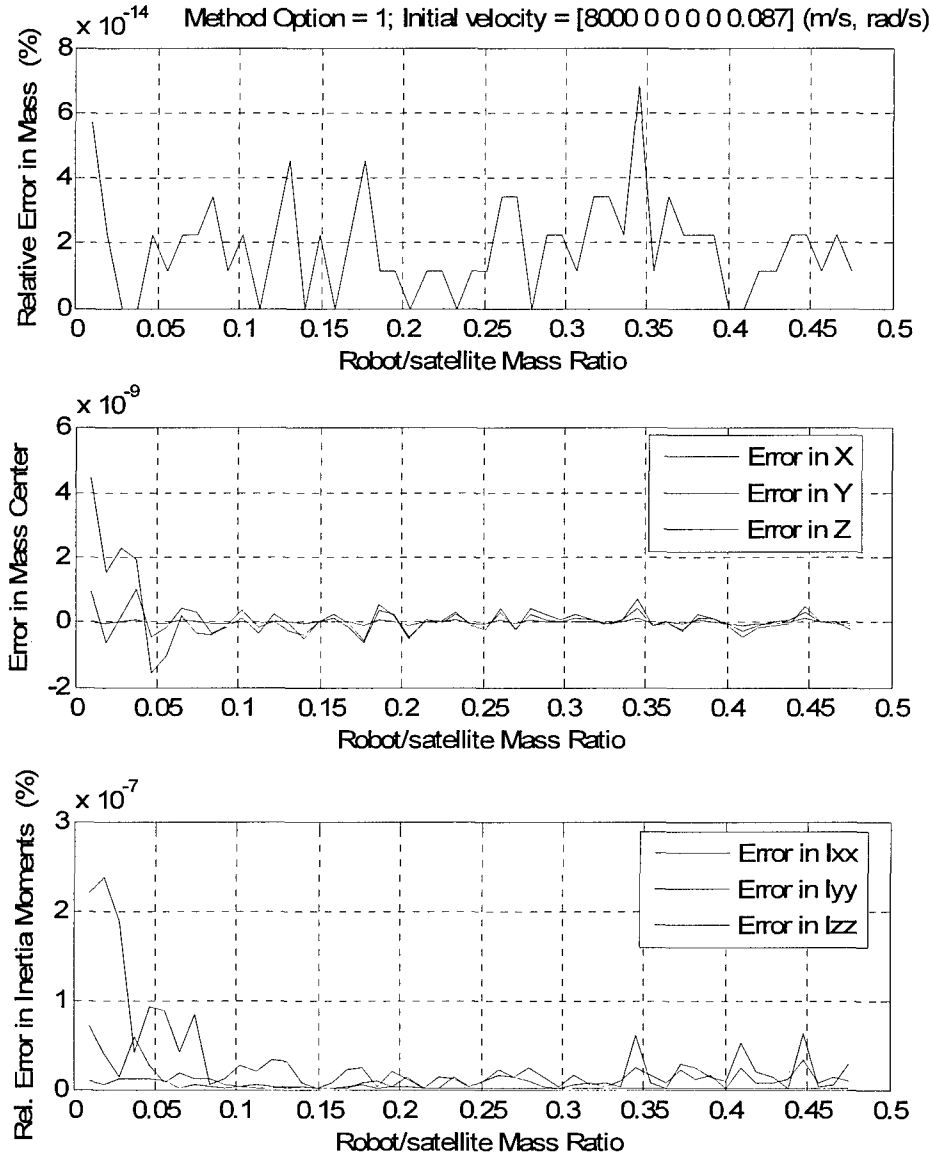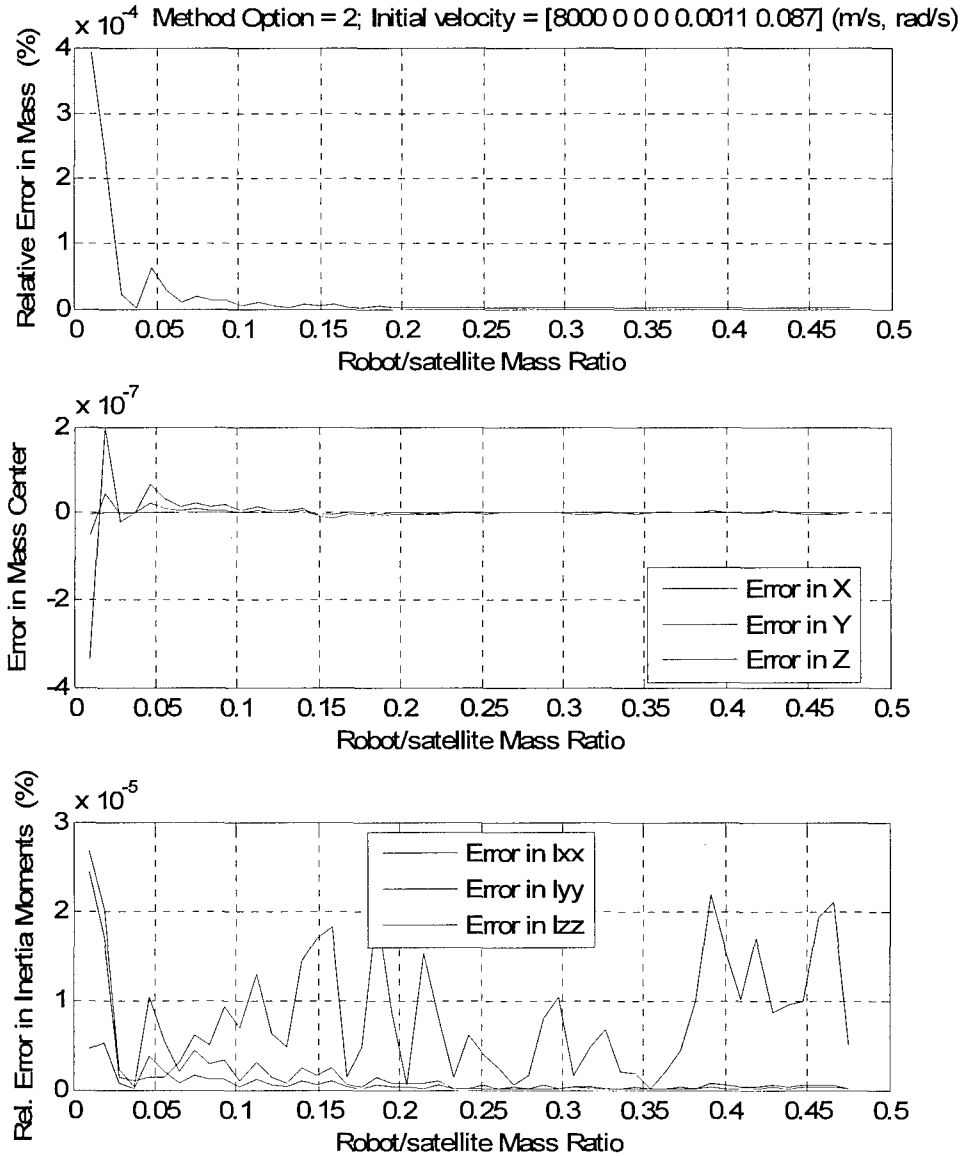

Fig.10 Identification errors for different arm-spacecraft mass ratio
(Note: the error in the position of the mass center is represented by the absolute error because the mass center is located at the origin and thus the relative error is undefined)

25

Example 3.2.2:

This example is the same as Example 3.2.1 except Option 2 is used to solve the identification problem where the initial momentum is assumed unknown and thus, the relative velocities are used in the process. The identification errors are plotted in Fig.11. As we can see, when the mass ratio is small, the resulting identification errors by using Option 2 is much larger that using Option 1. This tells us that we should use Option 1 to solve the identification problem if condition allows.

Fig.11 Identification errors for different arm-spacecraft mass ratio
(Note: the error in the position of the mass center is represented by the absolute error because the mass center is located at the origin and thus the relative error is undefined)

26

Example 3.2.3:

In this case the arm is commanded to go along the general trajectory B defined in Section 3.3 (see Fig.14). With this arm maneuver, an initial spinning about the Z axis only will not be enough to identify all the moments of inertia. Thus, a tiny initial rate about the Y axis is added to the initial velocity. The 0.0011 deg/s rate in Y axis is equivalent to the angular rate of a 90-min Earth orbit. The identification errors from Option 1 are plotted in Fig.12.
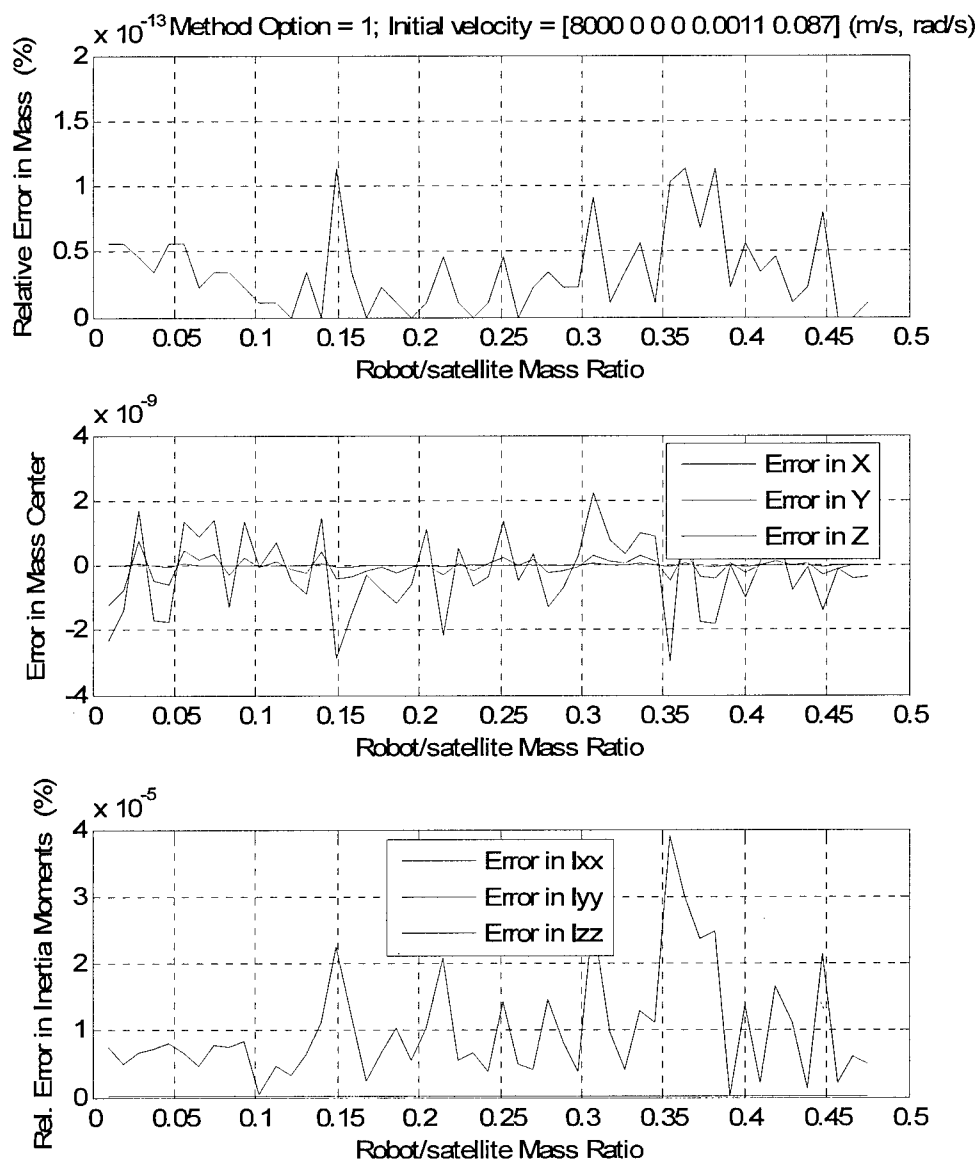

Fig.12 Identification errors for different arm-spacecraft mass ratio
(Note: the error in the position of the mass center is represented by the absolute error because the mass center is located at the origin and thus the relative error is undefined)

3.3 Effect of Arm Maneuvers

The method requires the robotic arm to move to different configurations in order to change the velocity of the spacecraft. It is then understandable that these configurations should be as different as possible in order to maximize the resulting new mass distribution and velocity variations. Moreover, to be able to identify all the components of the inertia tensor, the velocity changes must be in all directions. Therefore, the motion trajectory or path should span as large space as possible. In our investigation, four typical arm motion trajectories are defined for simulation tests. They are described below.

Trajectory A (see Fig.13)
It is the most general maneuver having the largest motion-span or arm maneuvering. The arm first stretches all the way upward; then it swings down to the horizontal plane while keeping fully stretched out; then it swings 360 degrees on horizontally. The starting configuration of the trajectory is $\theta = \begin{bmatrix} 0 & 0 & 0 & 0 & 0 & 0 \end{bmatrix}$ and the ending configuration is $\theta = \begin{bmatrix} 180° & -180° & 180° & -180° & 180° & 0° \end{bmatrix}$. A few typical configurations of the trajectory are shown in Fig.13. The figure also plots the time histories of the 3-D linear and angular velocities along the trajectory.

Trajectory B (see Fig.14)
This trajectory has the second largest motion-span or arm maneuvering. The arm is fully stretched out and swings in parallel to the top face of the satellite. The starting configuration of the trajectory is $\theta = \begin{bmatrix} 0 & 0 & 180° & -180° & 0 & 0 \end{bmatrix}$ and ending configuration is $\theta = \begin{bmatrix} 180° & 0 & 180° & -180° & 0 & 0 \end{bmatrix}$. The starting and ending configurations are shown in Fig.14. The figure also plots the time histories of the 3-D linear and angular velocities along the trajectory.

Trajectory C (see Fig.15)
This trajectory has the third largest motion-span or arm maneuvering. The arm stretches all the way up and then folds all the way down. The starting configuration of the trajectory is $\theta = \begin{bmatrix} 0 & 0 & 0 & 0 & 0 & 0 \end{bmatrix}$ and ending configuration is $\theta = \begin{bmatrix} 0 & -90° & 180° & -180° & 0 & 0 \end{bmatrix}$. The starting and ending configurations of the arm are shown in Fig.15. The figure also plots the time histories of the 3-D linear and angular velocities along the trajectory.

Trajectory D (see Fig.16)
This trajectory has the smallest motion-span or arm maneuvering. The arm is fully stretched upright and spin by the first joint (along the Z axis). The starting configuration of the trajectory is $\theta = \begin{bmatrix} 0 & -90° & 180° & -180° & 0 & 0 \end{bmatrix}$ and the ending configuration is $\theta = \begin{bmatrix} 180° & -90° & 180° & -180° & 0 & 0 \end{bmatrix}$, as shown in Fig.16. The figure also plots the time histories of the 3-D linear and angular velocities along the trajectory.
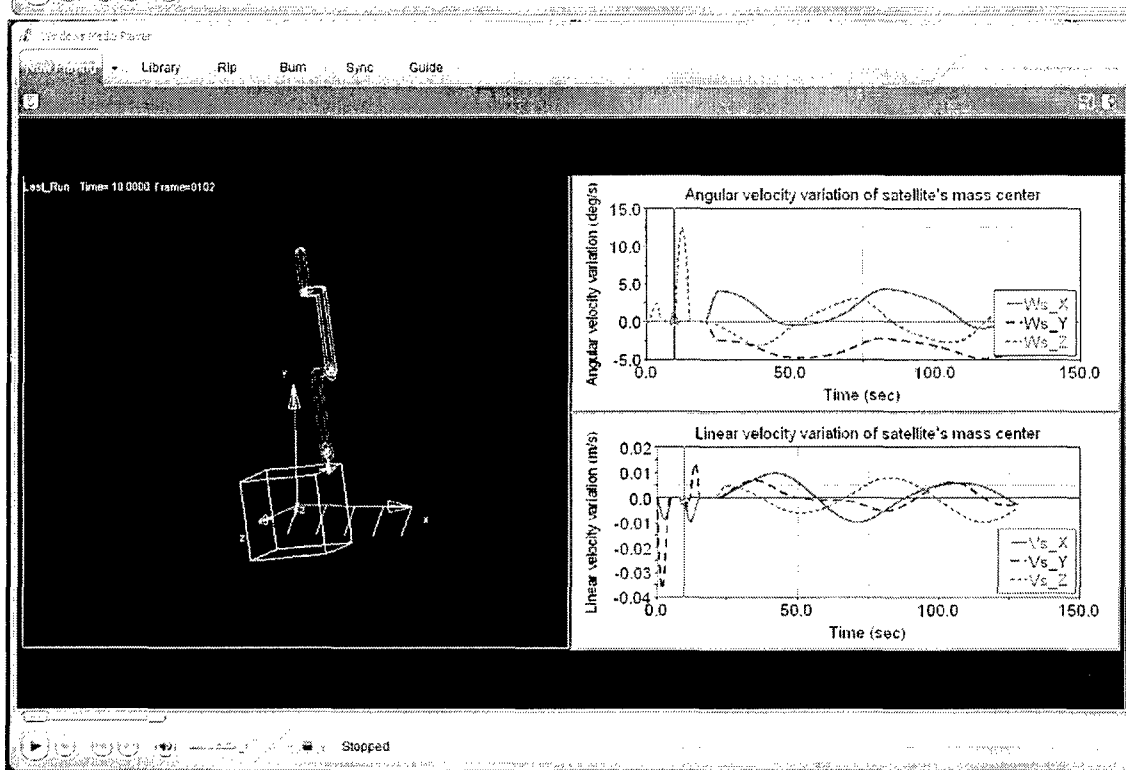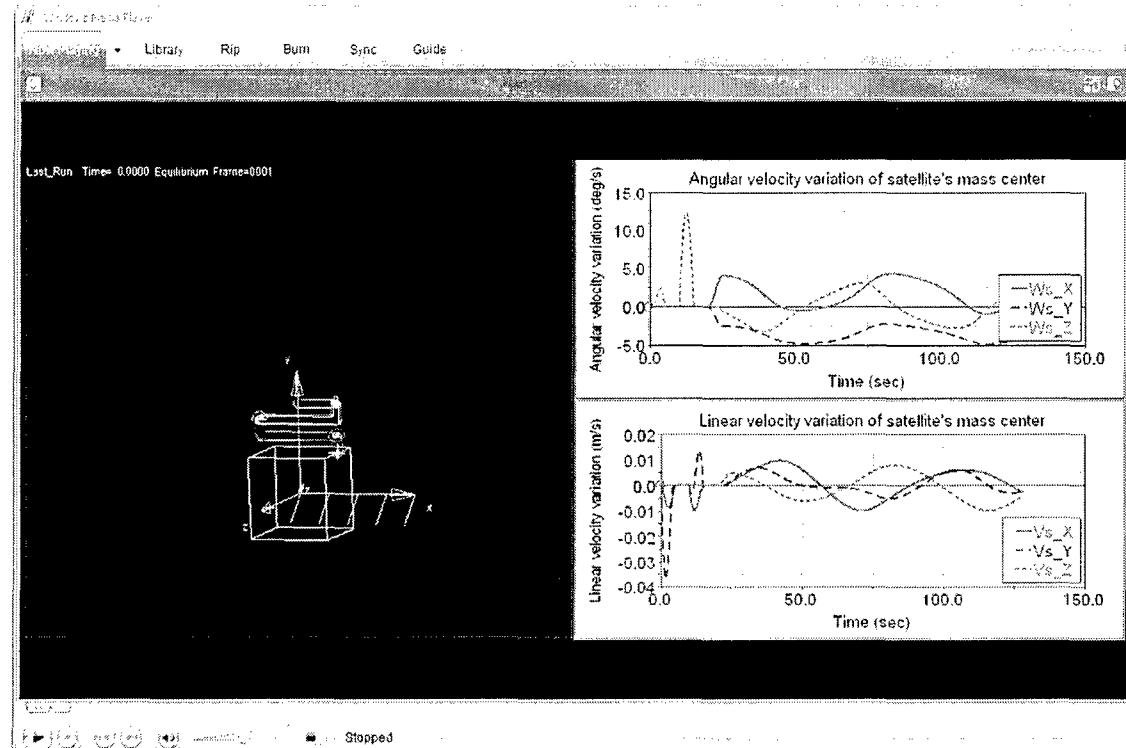
The velocity profiles associated with the above-mentioned trajectories give a good idea about how good they are for the identification. In general, a trajectory is good if it causes large velocity changes in all the 6 components when the arm moves along the trajectory, such as trajectory A. a trajectory is not good if one or more velocity components are not changed much along the trajectory, such as trajectory D.

Among the four typical trajectories, trajectory A is the best one for inertia identification because it has the largest motion span and trajectory D is the worst one because it has the smallest motion span. The other two trajectories are in the middle. This point can be seen from the example simulations presented in the next few subsections.

28

Trajectory A: The arm moves very generally

starting at Initial configuration: $\theta = \begin{bmatrix} 0 & 0 & 0 & 0 & 0 & 0 \end{bmatrix}$ and

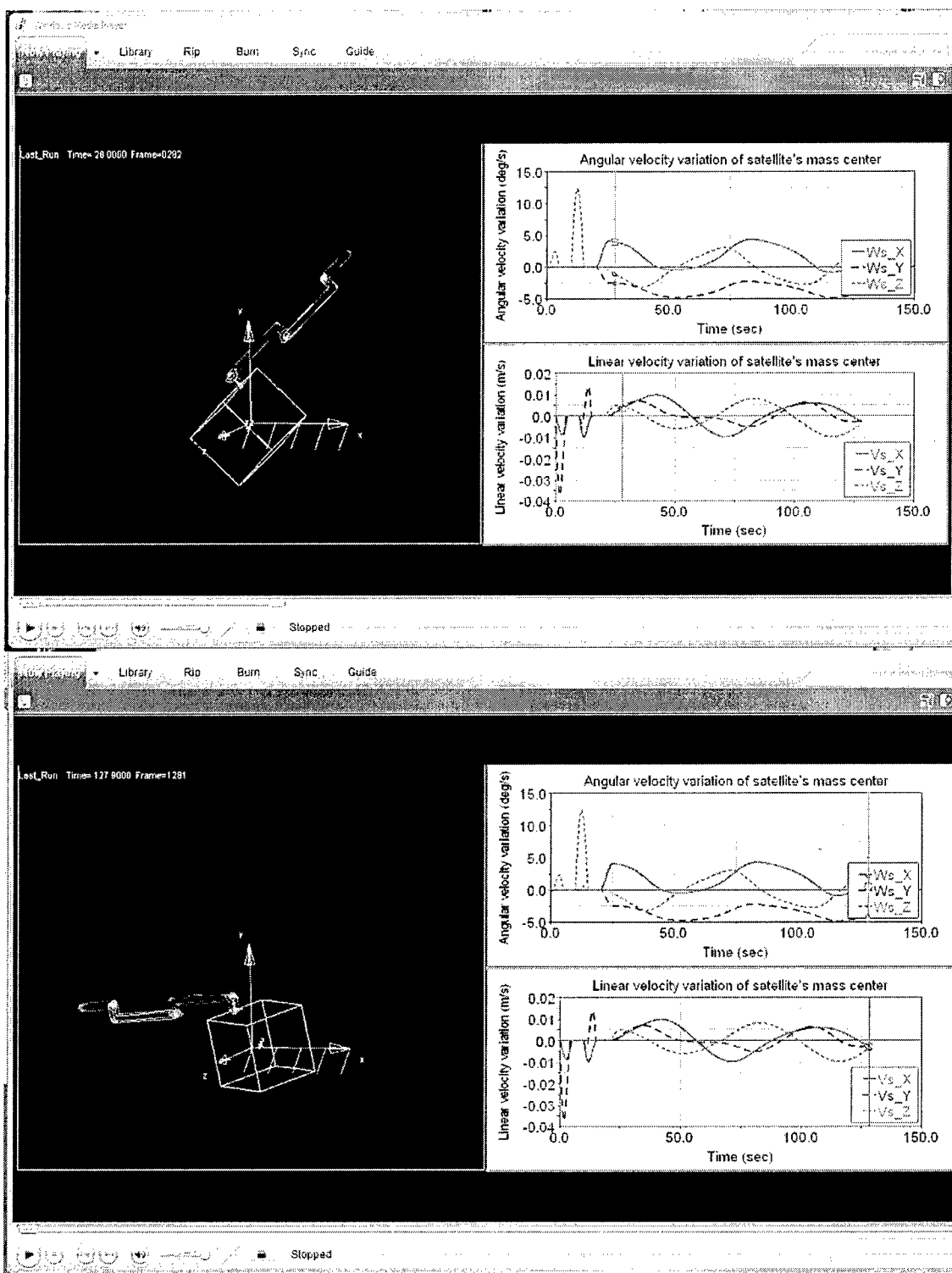ending at the configuration $\theta = \begin{bmatrix} 180° & -180° & 180° & -180° & 180° & 0° \end{bmatrix}$

Fig.13 The initial, two middle, and the ending configurations of trajectory A

Trajectory C: the arm is fully stretched out and swings horizontally

starting at Initial configuration: $\theta = \begin{bmatrix} 0 & 0 & 180° & -180° & 0 & 0 \end{bmatrix}$ and

ending at the configuration $\theta = \begin{bmatrix} 180° & 0 & 180° & -180° & 0 & 0 \end{bmatrix}$

Fig.14 The initial and final configurations of trajectory B

Trajectory C: the arm moves up and down vertically
starting at Initial configuration: $\theta = \begin{bmatrix} 0 & 0 & 0 & 0 & 0 & 0 \end{bmatrix}$ and
ending at the configuration $\theta = \begin{bmatrix} 0 & -90° & 180° & -180° & 0 & 0 \end{bmatrix}$
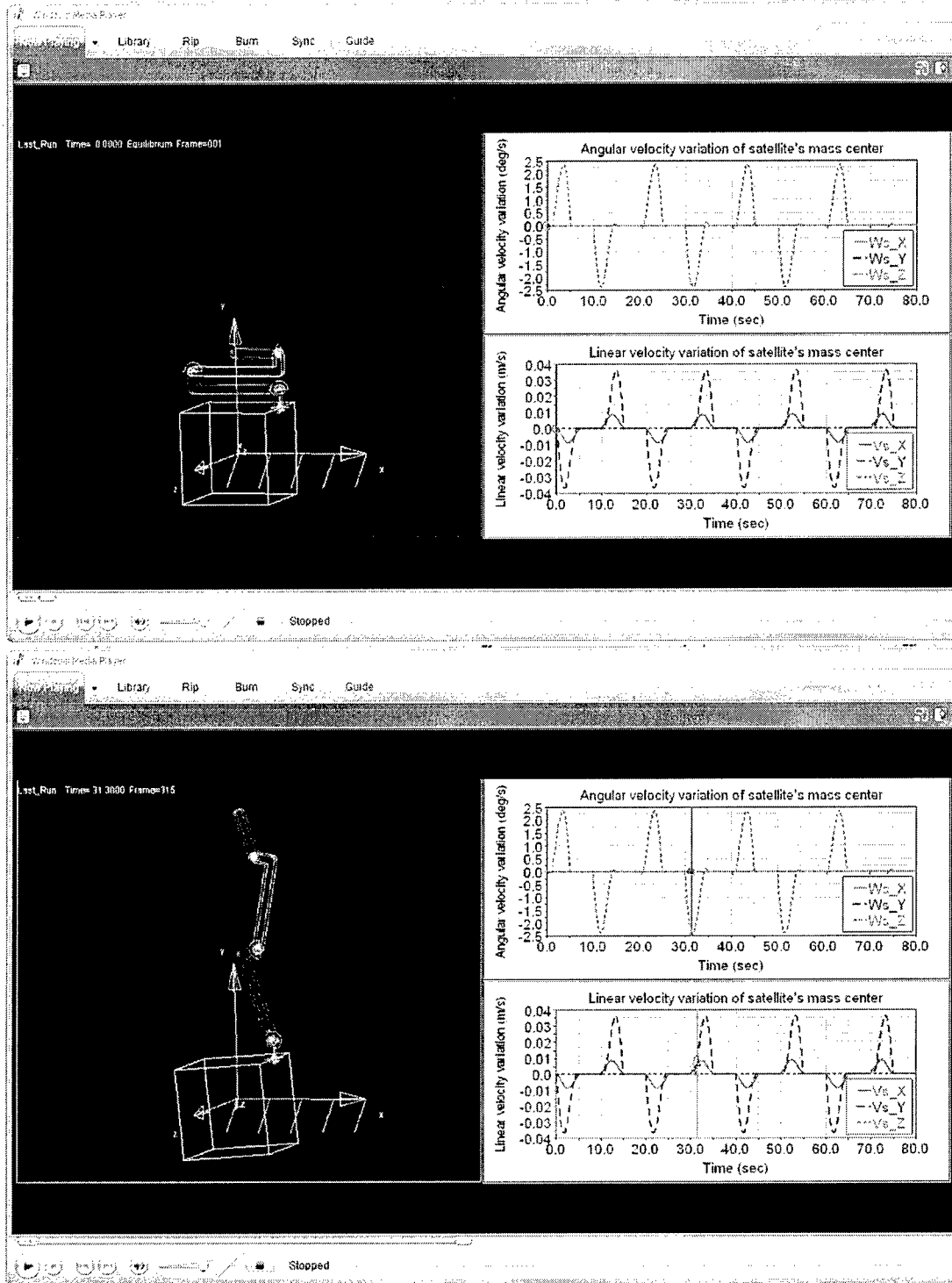

Fig.15 The initial and fully stretched-up configurations of trajectory C

32

Trajectory D: the arm is fully stretched out and swings horizontally
starting at Initial configuration: $\boldsymbol{\theta} = \begin{bmatrix} 0 & -90° & 180° & -180° & 0 & 0 \end{bmatrix}$ and
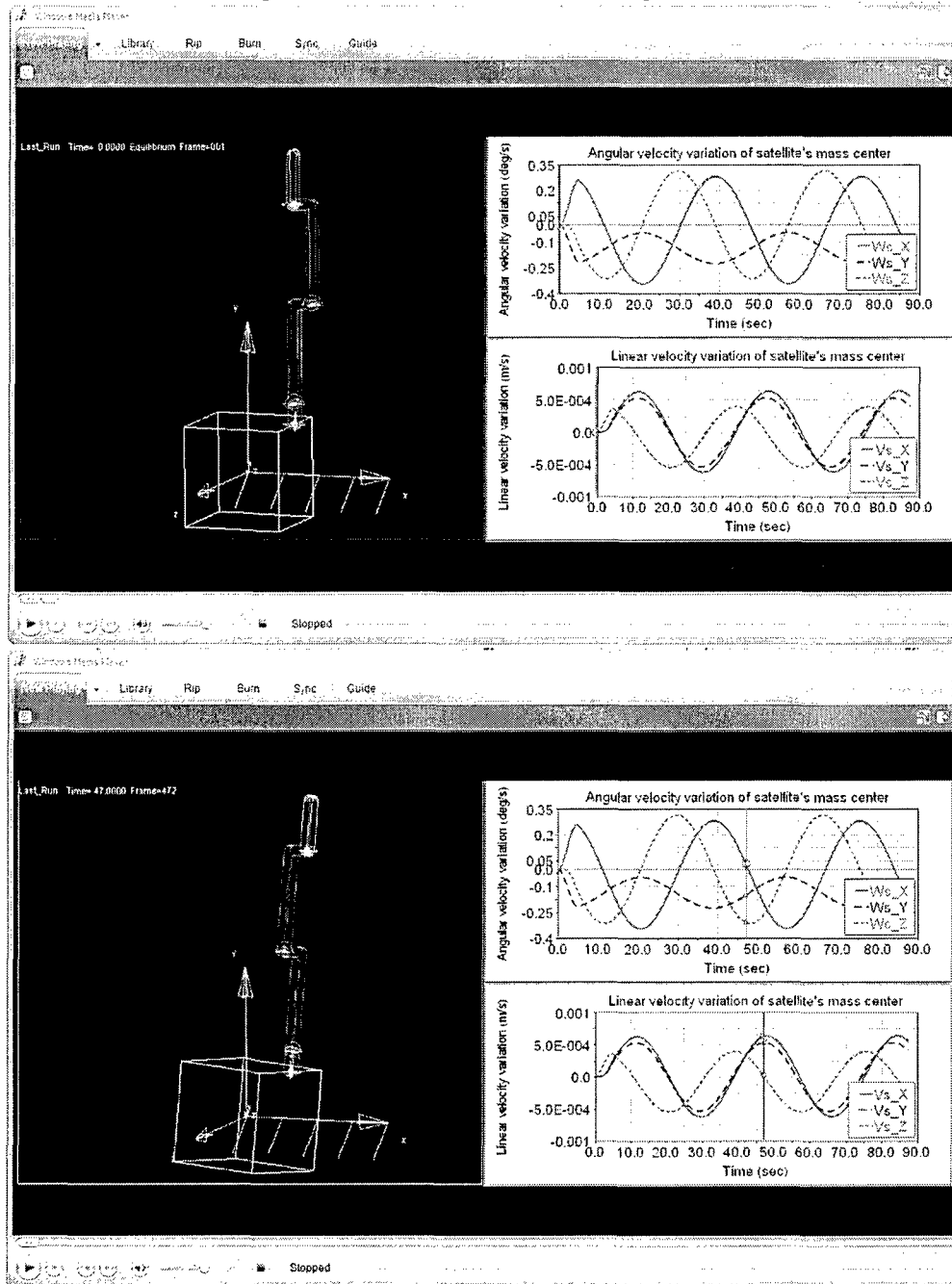ending at the configuration $\boldsymbol{\theta} = \begin{bmatrix} 180° & -90° & 180° & -180° & 0 & 0 \end{bmatrix}$

Fig.16 The initial and final configurations of trajectory D

33

3.4 Sensitivity to Bias in Velocity Measurements

Velocity measurements always have errors which will cause corresponding errors in the identification results. To access the sensitivity to the measurement bias, a few examples are illustrated in this section. In all examples, ten velocity measurements are taken at the configurations equally separated along the path defined in each example. A bias error (defined as percentage of the true velocity value) is added to the measured linear velocity or angular velocity (but not both). The corresponding errors in the identified parameters are computed and plotted. The plotted identification errors are defined as the differences between the identified values of the inertia parameters and the true values of the same inertia parameters.

The plots show that the errors in the identified inertia parameters caused by the measurement bias error are negligible. The error in the identified position of mass center is also very small. The errors in the moments and products of inertia are less than 1/5 of the measurement bias error, which are also considered small. This clearly indicates that the measurement bias is not a concern for the proposed identification method.

Example 3.4.1:

The arm is commanded to go along the general trajectory A defined in Section 3.3 (see Fig.13). The spacecraft body is initially spinning about the Z axis at a rate of 1.0 deg/s. The identification errors are plotted in Figs.17-18.
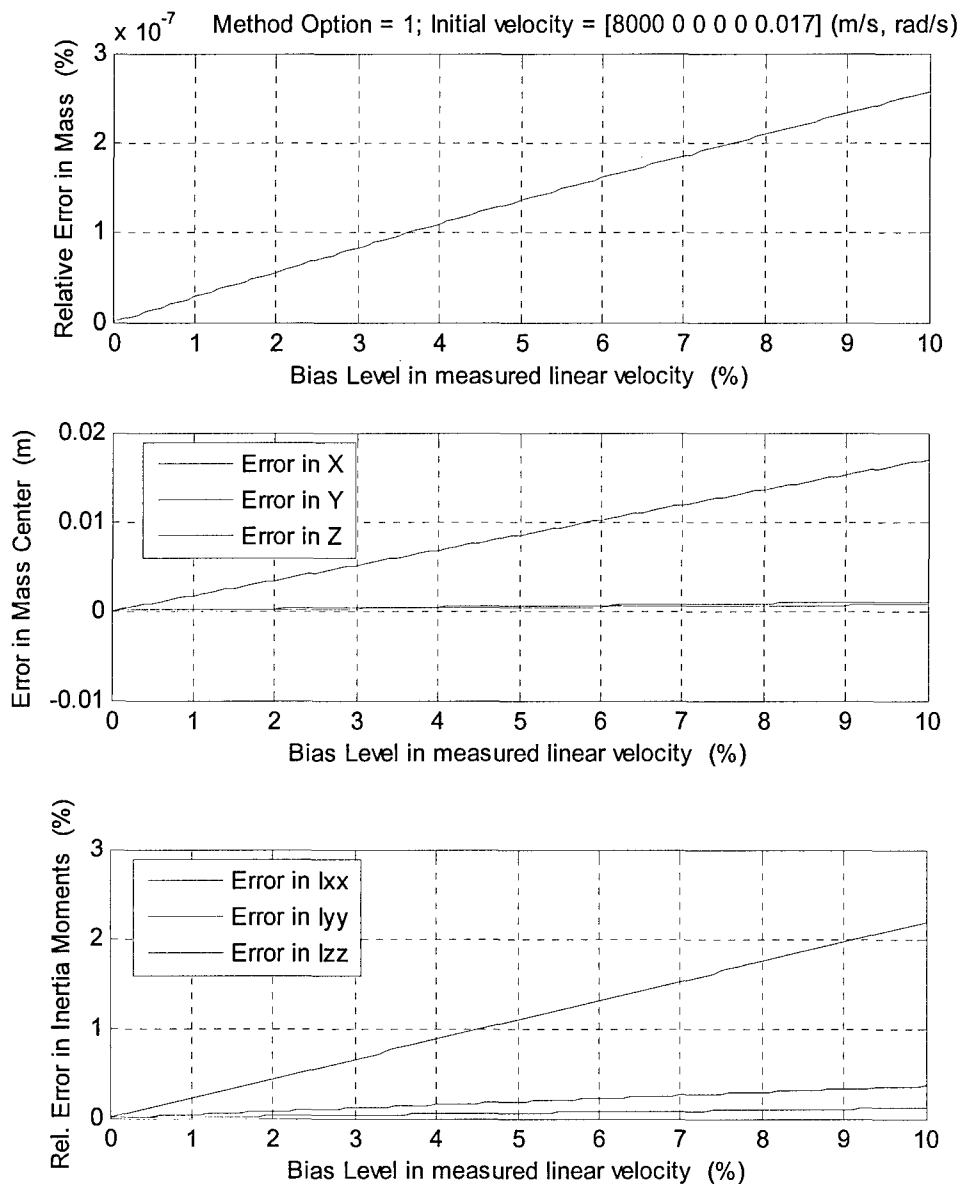

Fig.17 Identification errors when different bias errors are added to the linear velocity

(Note: the error in the position of the mass center is represented by the absolute error because the mass center is located at the origin and thus the relative error is undefined)
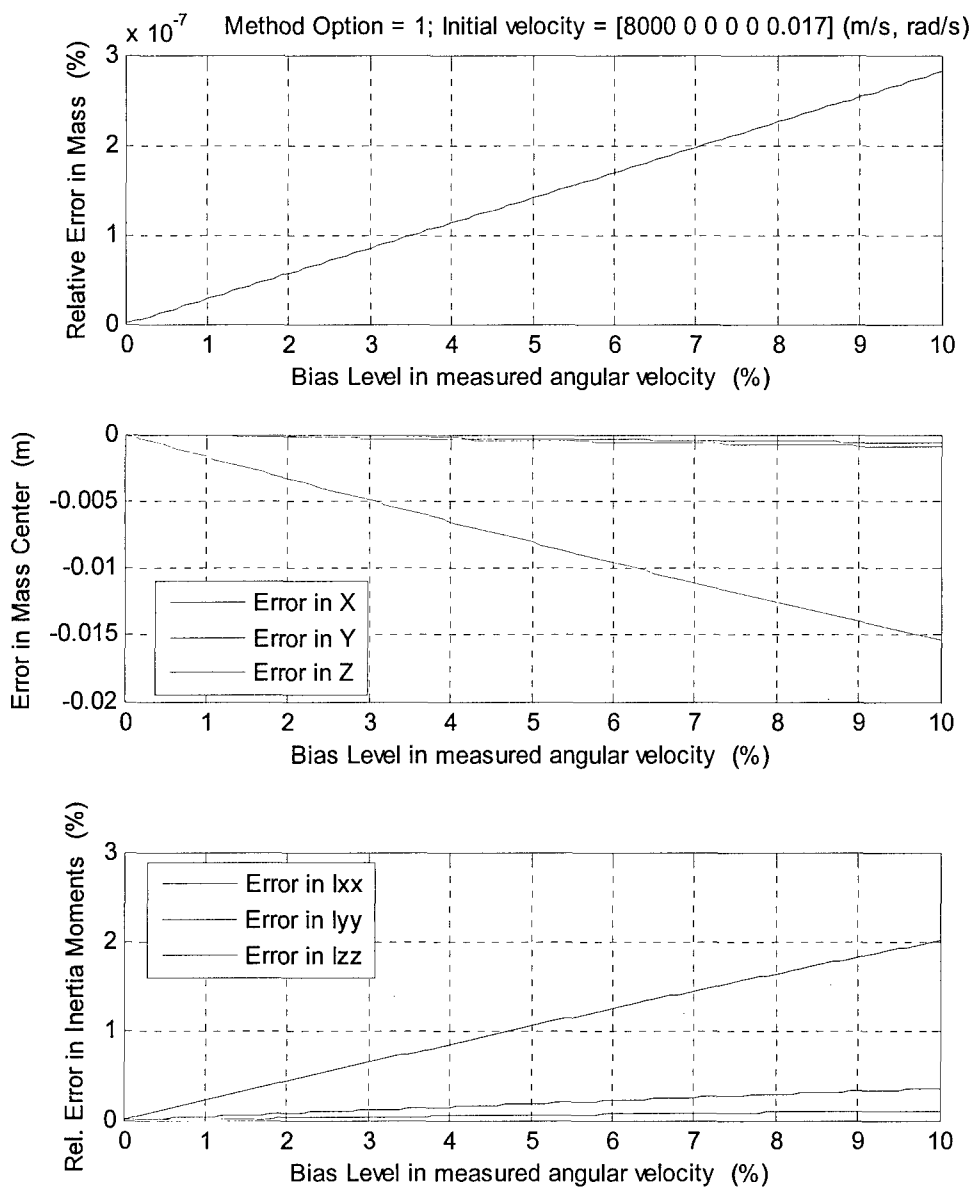
Fig.18 Identification errors when different bias errors are added to the angular velocity
(Note: the error in the position of the mass center is represented by the absolute error because the mass center is located at the origin and thus the relative error is undefined)

Example 3.4.2:

In this example, the arm is fully stretched out and swings in the horizontal plane along the trajectory C defined in Section 3.3 (see Fig.15). The spacecraft body is initially rotating at a rate of 1.0 deg/s about the Y axis (pitch) and 5.0 deg/s about the Z axis (yaw). The identification errors are plotted in Fig.19.
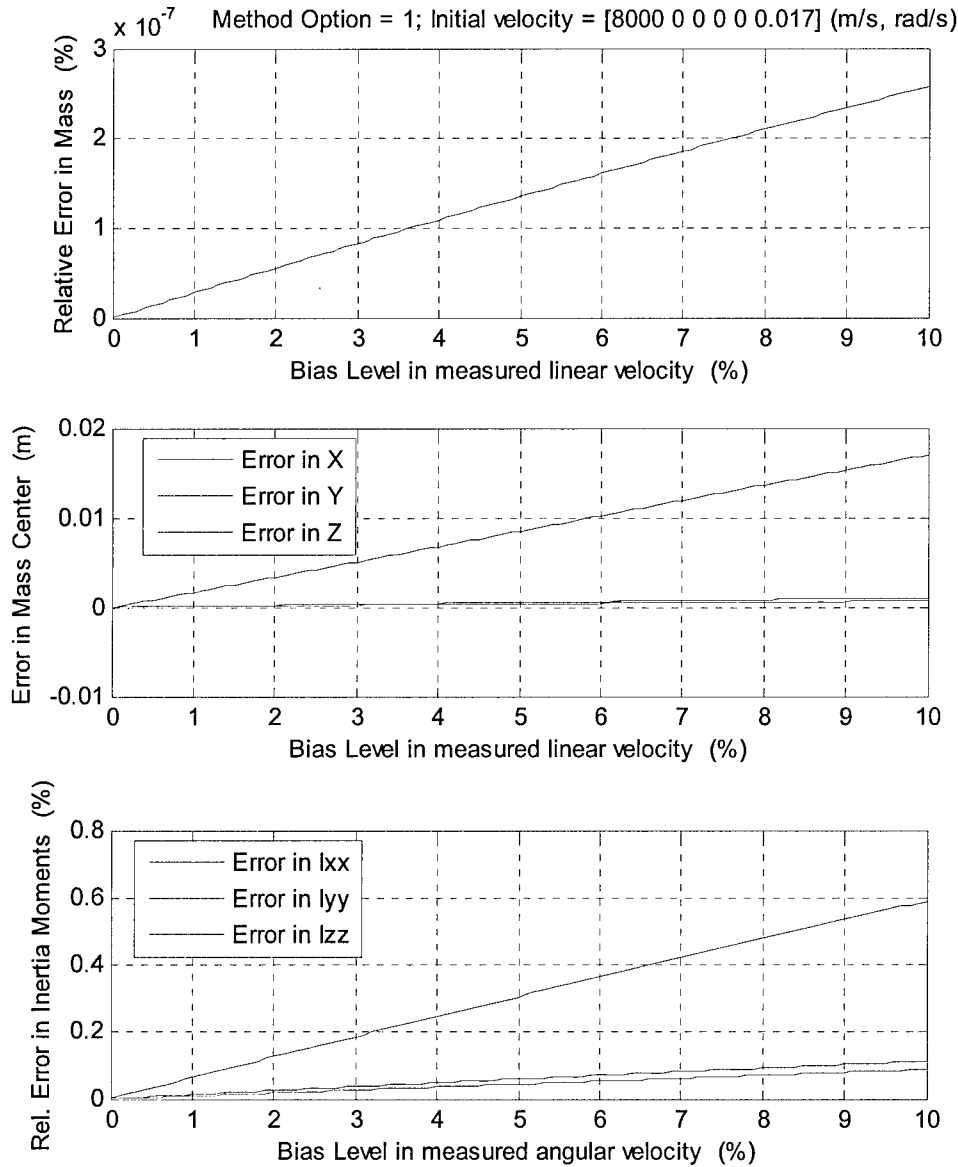

Fig.19 Identification errors when different bias errors are added to the angular velocity

3.5 Sensitivity to Sensor Noise

Velocity measurements always have errors due to sensor noise. These random errors will cause corresponding errors in the identification results. To access the sensitivity to the sensor noise, a few examples are illustrated in this section. In all examples, ten velocity measurements are taken at the configurations equally separated along the path defined in each example. A random error (with zero mean and the standard deviation defined as a percentage of the true velocity value) is added to each of the measured velocity component and then the corresponding errors in the identified parameters are computed.

Simulation tests with the four trajectories all show that the random errors in velocity data can cause significant errors in identified inertia parameters. For the four different arm maneuvering trajectories, the identification errors continuously increases from trajectory A to trajectory D, with A having the minimum errors and D having the maximum errors. This is mainly because, as discussed in Section 3.2, trajectory A has the largest arm maneuvering and trajectory D has the minimum arm maneuvering. If we can control the velocity-measurement errors within 3% level, the resulting identification errors will also be more or less about 3% level for trajectory A. However, the same 3% measurement errors could cause over 200% identification errors if using trajectory D. This is totally unacceptable. Therefore, we know that selection of arm maneuvering trajectory for the identification process is very important.

For the same trajectory, the errors in identified mass and mass center seems to be less than that in the inertia tensor. In other words, identification of inertia tensor is more sensitive to sensor noise than that of mass and mass center.

<u>Example 3.5.1:</u>

The arm is commanded to go along the general trajectory A defined in Section 3.3 (see Fig.13). The spacecraft body is initially spinning about the Z axis at a rate of 1.0 deg/s. The identification errors are plotted in Fig.20.
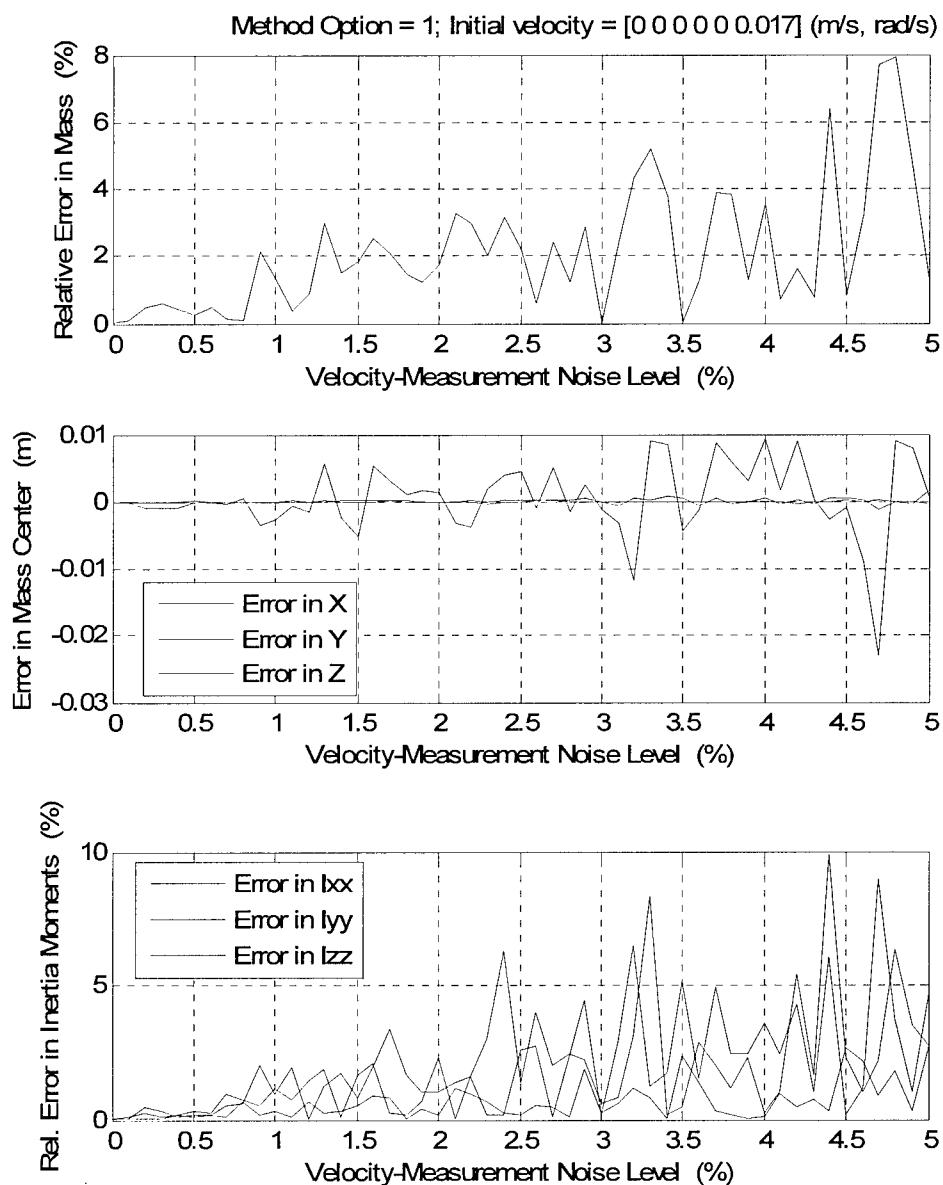

Fig.20 Identification errors when different noises are added to the angular velocity measurement (Note: the error in the position of the mass center is represented by the absolute error because the mass center is located at the origin and thus the relative error is undefined)

Example 3.5.2:

In this example, the arm is fully stretched out and swings in the horizontal plane along the trajectory B defined in Section 3.3 (see Fig.14). The spacecraft body is initially rotating at a rate of 1.0 deg/s about the Y axis (pitch) and 5.0 deg/s about the Z axis (yaw). The identification errors are plotted in Fig.21.
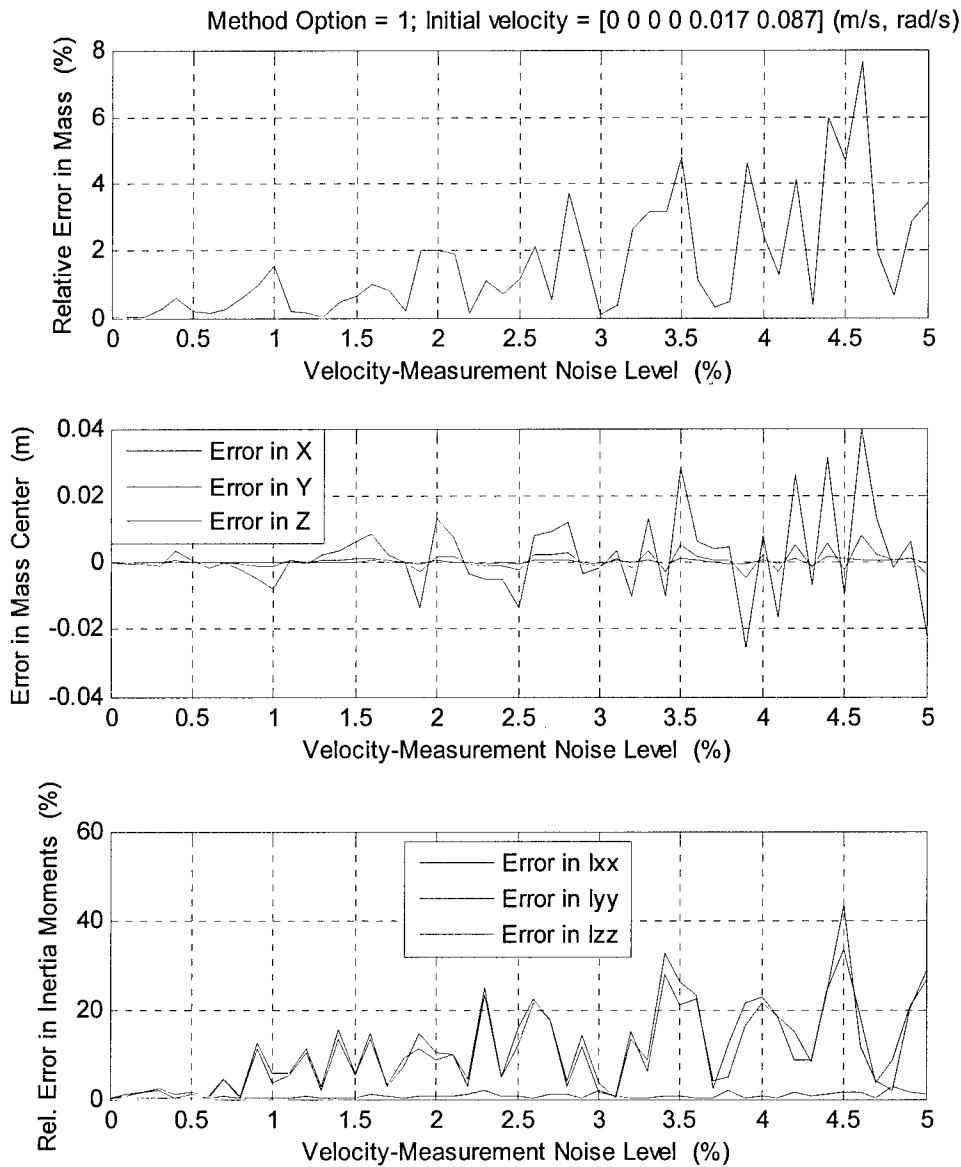

Fig.21 Identification errors when different noises are added to the angular velocity measurement

Example 3.5.3:

In this example, the arm is fully stretched out and swings in the horizontal plane along the trajectory C defined in Section 3.3 (see Fig.15). The spacecraft body is initially rotating at a rate of 1.0 deg/s about the Y axis (pitch) and 5.0 deg/s about the Z axis (yaw). The identification errors are plotted in Fig.22.

Fig.22 Identification errors when different noises are added to the angular velocity measurement

41

Example 3.5.4:

In this example, the arm is spinning when it is fully stretched out and upright along the trajectory D defined in Section 3.3 (see Fig.16). The spacecraft body is initially rotating at a rate of 1.0 deg/s about the Y axis (pitch) and 5.0 deg/s about the Z axis (yaw). The identification errors are plotted in Fig.23.
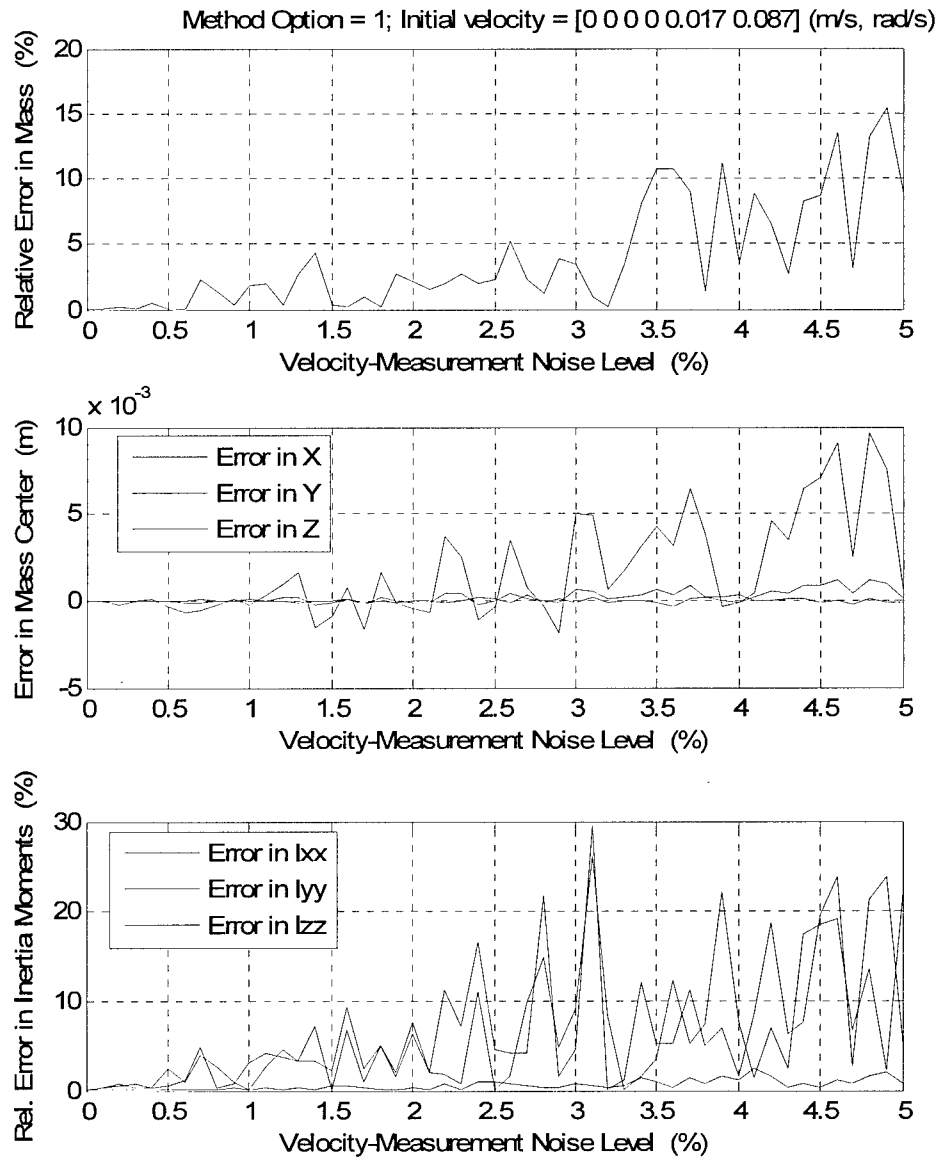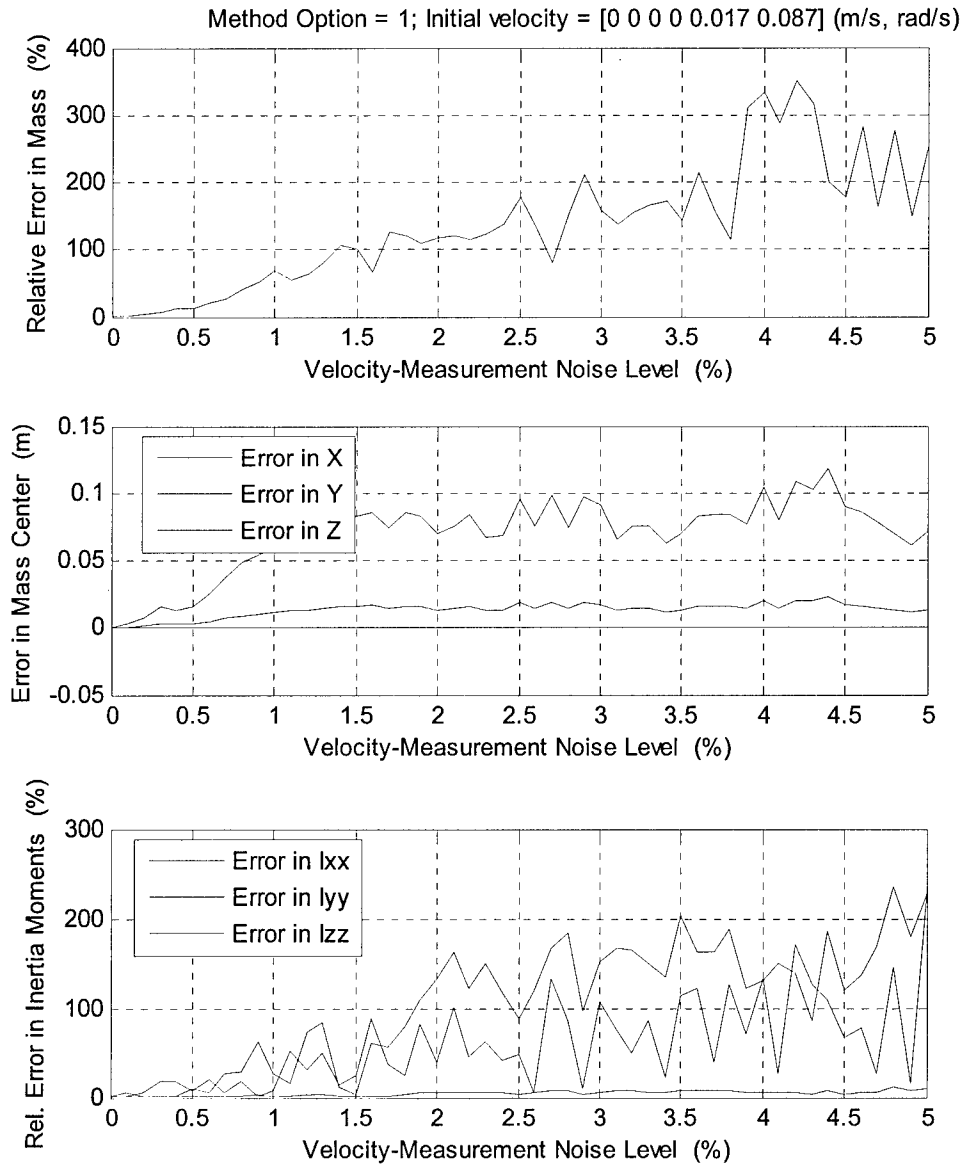

Fig.23 Identification errors when different noises are added to the angular velocity measurement (Note: the error in the position of the mass center is represented by the absolute error because the mass center is located at the origin and thus the relative error is undefined)

3.6 Effect of Gravity-Gradient Torque

Not investigated (due to time and funding limitations)

3.7 A Study of the Case using Solar-Array Mechanisms

Dr. Robertson and Dr. Pham of AFRL asked if the robotics-based identification method can be extended to more general cases where other onboard mechanisms (as opposed to just robotic arms) can be used to identify the inertia properties. These mechanisms may include solar arrays, antennas, momentum wheels, etc. If this question gets a positive answer, then the impact of the identification method will be much larger because the method will no longer rely on a robotic arm. To fully answer this question, an intensive research is needed which is beyond the scope of this short-term research project. In this section, we perform a preliminary study of the possibility of using a solar array for inertia identification just for gaining some idea about the outcome of this extended research.

For the simulation study, we modify the system dynamics model defined in 3.1 by replacing the robotic arm with two solar panels. The two solar arrays are identical and symmetrically attached to the spacecraft body, as shown in Fig.24. Each array is a 2-DOF mechanism for tracking the Sun. The mechanical parameters of the arrays are given in Table 2.
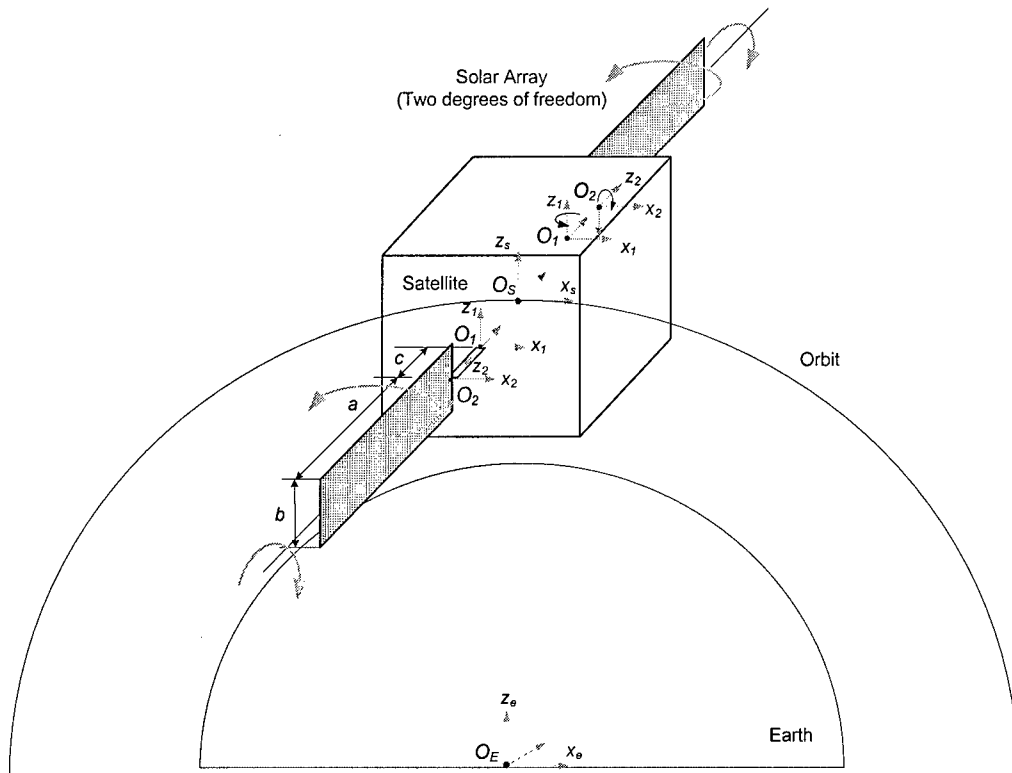

Fig.24 Reference frames of the spacecraft with sun-tracking solar arrays (in home configuration)

43

Table 2 Kinematics and Dynamics Parameters of the Spacecraft with Solar Arrays

Body	Parameters	Unit	Value	Note
Spacecraft	a_s, b_s, c_s	m	1.0, 1.0, 1.0	
	m_S	kg	1000.0	
	$^S\mathbf{c}_S$	m	$\begin{bmatrix} 0 & 0 & 0 \end{bmatrix}^T$	
	$^S\mathbf{I}_S$	kg·m^2	$I_{xx} = I_{yy} = I_{zz} = (1/6)m_S a_S^2$	
Solar Array 1	a, b, c	m	2.0, 1.0, 0.2	
	m_A	kg	50	(5% spacecraft mass)
	$^1\mathbf{c}_1$	m	$\begin{bmatrix} 0 & a_1/2 + c_1 & 0 \end{bmatrix}^T$	
	$^1\mathbf{I}_1$	kg·m^2	$\dfrac{1}{12}m_A \, \mathrm{diag}(a^2 + b^2, a^2, b^2)$	Calculated from geometry
Solar Array 2	a, b, c	m	2.0, 1.0, 0.2	
	m_A	kg	50	(5% spacecraft mass)
	$^2\mathbf{c}_2$	m	$\begin{bmatrix} 0 & -a/2 - c & 0 \end{bmatrix}^T$	
	$^2\mathbf{I}_2$	kg·m^2	$\dfrac{1}{12}m_A \, \mathrm{diag}(a^2 + b^2, a^2, b^2)$	Calculated from geometry

Simulation tests showed that, by using the solar arrays, all the inertia parameters of the satellite can be identified precisely without any problems if the velocities of the satellite can be precisely measured. However, similarly as in the cases of using a robotic arm, if the velocity data has errors or sensor noise, the identified inertia parameters will also have errors. Two simulation examples are included in the next few pages to demonstrate this.

The simulations examples suggest that the identification of the mass and mass-center location is not sensitive to sensor noise but the identification of inertia tensor is very sensitive to sensor noise. Therefore, in order to make the method practically feasible, we need to either reduce the sensitivity of the method to sensor noise or directly reduce the velocity measurement errors.

Example 3.7.1:

In this example, the two solar arrays are spinning about their own axes by 180 degrees. In other words, the joint angles are from $\theta = \begin{bmatrix} 0 & 0 \end{bmatrix}$ to $\theta = \begin{bmatrix} 0 & 180° \end{bmatrix}$ for each solar panel. Ten velocity measurements are taken at the configurations equally separated along the path. The spacecraft body is initially rotating at 1.0 deg/s about the Y axis and also 1.0 deg/s about the Z axis. Based on the velocity data, the inertia parameters of the spacecraft are identified. The identification errors are plotted in Fig.25. As one can see, the errors in mass and mass centers are negligible but these in inertia tensor are very large. This is because the angular maneuvering of the satellite caused by the solar arrays is not large enough. Therefore, we can say that the identification of inertia tensor is very sensitive to sensor noise.
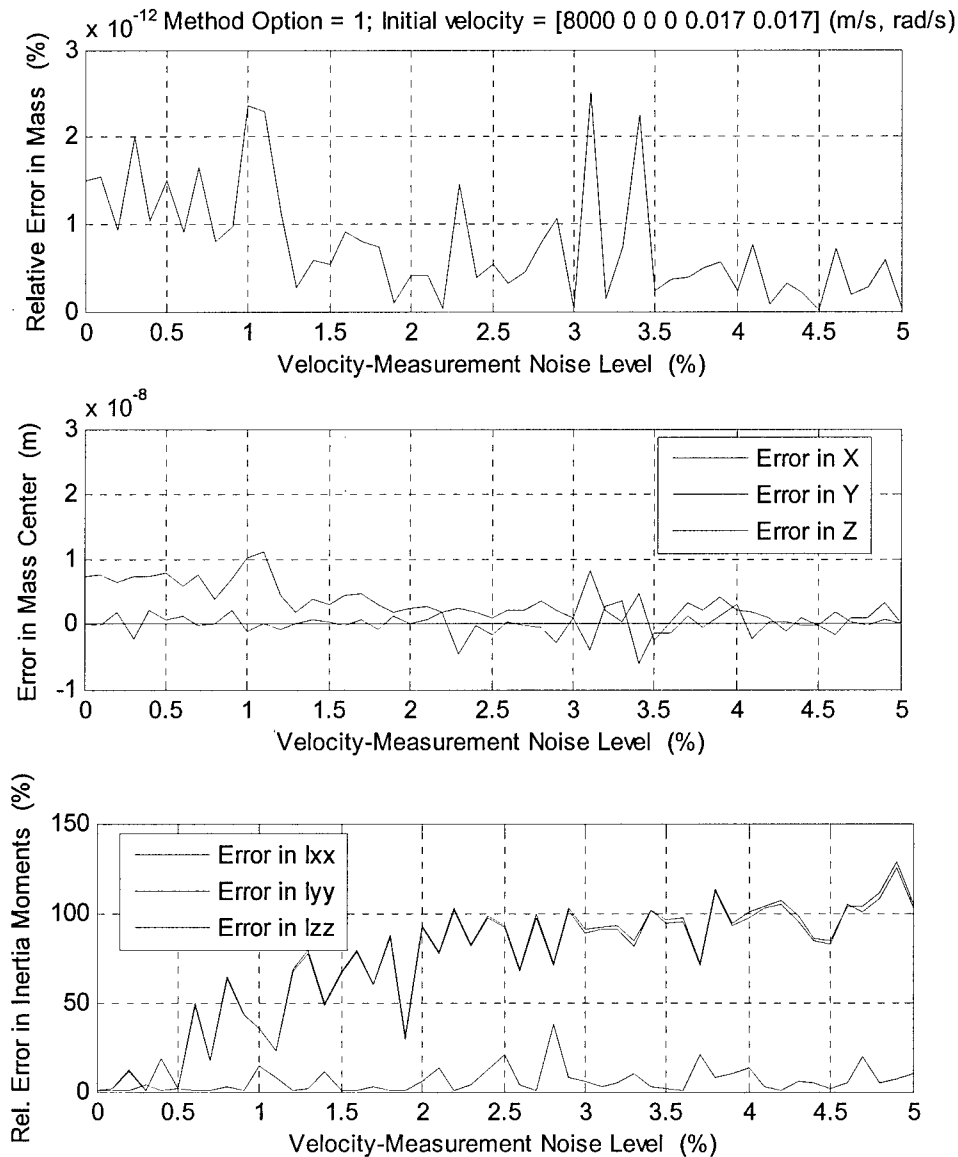

Fig.25 The identification errors versus the velocity measurement noise level
(Note: the error in the position of the mass center is represented by the absolute error because the mass center is located at the origin and thus the relative error is undefined)

45

Example 3.7.2:

In this example, the two solar arrays are spinning about their own axes by 180 degrees. In other words, the joint angles are from $\theta = \begin{bmatrix} 0 & 0 \end{bmatrix}$ to $\theta = \begin{bmatrix} 30° & 180° \end{bmatrix}$ for each solar panel. Ten velocity measurements are taken at the configurations equally separated along the path. The spacecraft body is initially rotating at 1.0 deg/s about the Y axis and also 1.0 deg/s about the Z axis. Based on the velocity data, the inertia parameters of the spacecraft are identified. The identification errors are plotted in Fig.26. As one can see, the errors in mass and mass centers are negligible but these in inertia tensor are very large. This is because the angular maneuvering of the satellite caused by the solar arrays is not large enough. Therefore, we can say that the identification of inertia tensor is very sensitive to sensor noise.
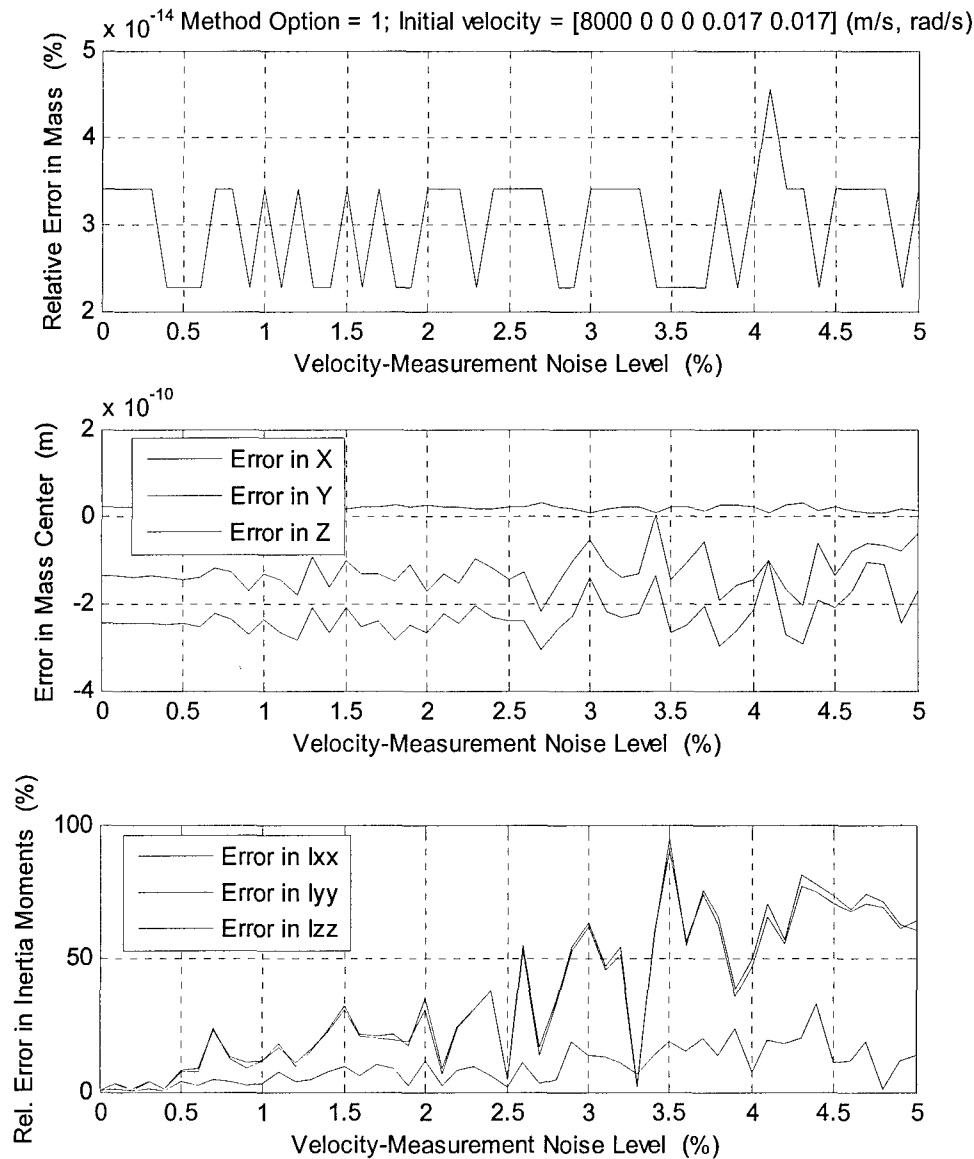

Fig.26 The identification errors versus the velocity measurement noise level

46

4. IDEA FOR EXPERIMENTAL VERIFICATION

Although an experimental study of the proposed technology is beyond the cope of this short-term project, an idea of testing the technology in a lab environment is presented in this section for discussion. The idea is illustrated in Fig.27.
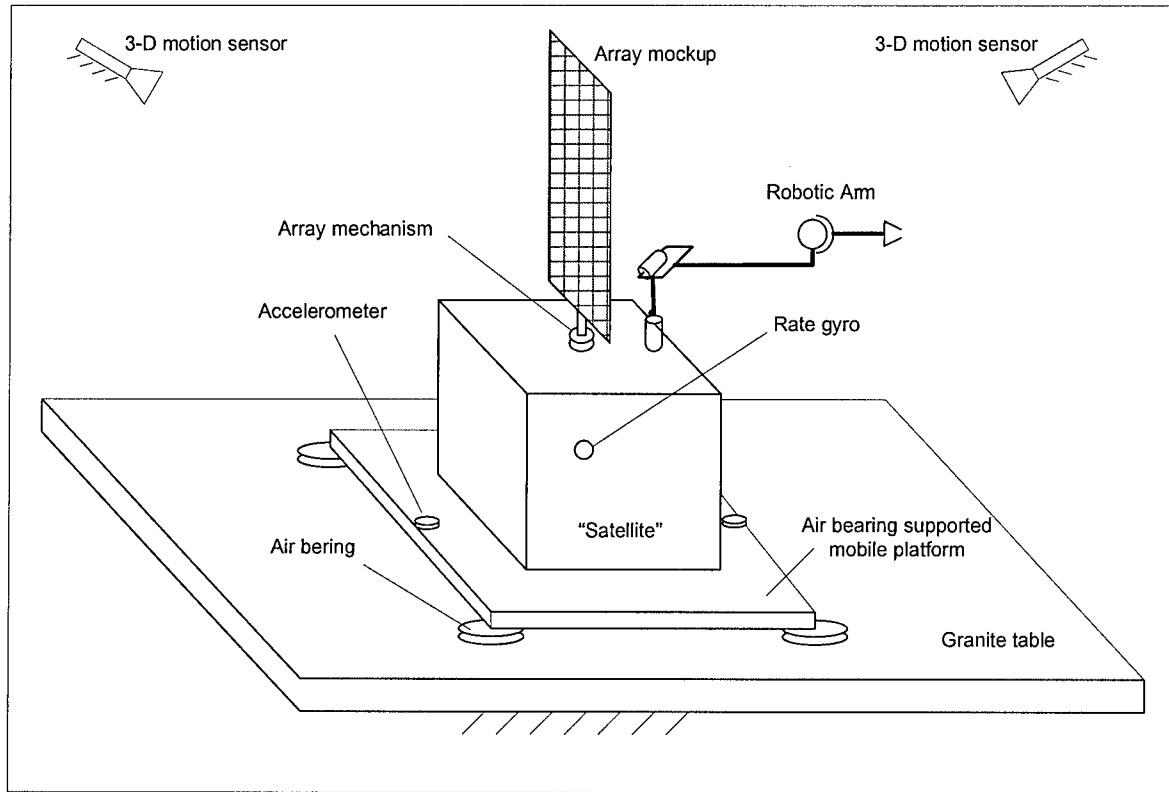

Figure 27 Concept of the a 2-D experiment testbed for testing the proposed technology

The testbed consists of a granite table, an air-bearing supported mobile frame, a spacecraft mockup, a robotic arm, and a 2-D motion sensing system. Note that the motion of each robot link including the end-effector does not need to be measured because it can be calculated from the well controlled joint motions instead. It leaves that only the motion of the spacecraft mockup or the mobile platform needs to be measured. Since this is can be considered as a rigid-body motion in the horizontal plane, it is not difficult to measure. We have several options: 1) use a visual sensor to track the position of the mobile frame and then estimate the velocities by differentiating the position data (results may be noisy and thus requiring filtering); 2) use two to three accelerometers to measure the accelerations of some specific points of the mobile frame and then, estimate the velocity by integrating the acceleration data; 3) use a rate gyro to measure angular velocity directly but the linear velocity still has to be measured by a visual sensor or accelerometers. Since the negligible friction between the air bearings and the granite table, the spacecraft and the robotic arm will behave like free floating on the top of the granite table. This will approximate a 2-D (3 degrees of freedom) free floating condition in the space.

In the experiment, we give a slight push to the mobile frame in order to generate an initial motion (sliding and/or spinning). Then, we command the robot to go through a series of new configurations and measure the linear and angular velocities at each of these new configurations. If we use visual position sensors, the

velocity can be estimated by differentiating the measured position data (the results may be noisy). If we use accelerometers, the velocity can be estimated by integrating the acceleration data. Rate gyro can direct measure angular velocity.

Since this is a 2D experimental system, we can identify only 4 out of the 10 inertia parameters of the spacecraft mockup. The identifiable parameters are the mass, the x and y coordinates of the mass center, and the second moment of inertia about the z axis. However, this should be enough to prove the principle of the proposed identification method and assess the feasibility and performance of the proposed technology.

An important requirement for the testbed is that the inertia properties of the robotic arms and the mobile platform must be known in advance. This is also a condition of the proposed inertia identification method in a real application mission. This requirement will not be difficult to meet because the hardware components are specially designed, manufactured, and integrated in the lab. We can always carefully measure and verify these properties of the hardware in the lab.

5.   CONCLUSIONS AND RECOMMENDATION

The following have been accomplished in this short project:

a) Developed the method of using an onboard robotic arm (or arms) to identify the inertia parameters of a flying spacecraft. Two variations of the method are proposed; one requires measuring both linear and angular velocities and the other requires measuring the angular velocity only. The latter is a nonlinear parameter identification problem and thus, much more difficult to solve. The focus of this project is on the former only.

b) Implemented a simulation model on ADAMS and data analysis program on Matlab to support the research. The simulation model consists of a rigid spacecraft and a 6-DOF rigid robotic arm.

c) Performed a series of simulations to test the new method for some basic concerns such as robustness, accuracy, and limitations.

d) Explored the idea of using a pair of solar arrays (instead of a robotic arm) to identify the same inertia parameters.

e) Proposed a concept of experimental verification of the proposed method in lab environment.

From the simulation tests, the following findings are concluded:

1) The method of using an onboard robotic arm to identify the inertia properties of a flying spacecraft is feasible in theory (note: "in theory" because it has not been experimentally verified).

2) The idea of using solar arrays (instead of a robotic arm) to identify the inertia properties of a spacecraft is also possible in theory.

3) In order to treat the problem as a linear identification problem (much easier to solve), it has to be formulated in two steps (or two sub-problems). The first step is to identify the mass and mass center of the spacecraft; and the second step is to identify the inertia tensor of the spacecraft.

4) The spacecraft does not require an initial spin (or rotation) for identifying the mass and mass center. However, it does require an initial spin (or rotation) to identify the inertia tensor. This initial angular velocity can be unknown (i.e., Option 2 of the method).

5) When using a robotic arm for inertia identification, note the following:

   – For good identification performance, the arm mass should be no less than 5~10% of the spacecraft mass.

   – The arm does not necessarily need 6 degrees of freedom. However, more degrees of freedom will make the required maneuvering easier.

   – If the spacecraft initially rotates about one axis only, then the arm motion should span at least two axes. If the spacecraft initially rotates in two axes, the arm motion can span only one axis.

   – The identification solution is not sensitive to (velocity) measurement bias, e.g., 10% bias causing less than 1% identification error.

   – The identification solution is sensitive to (velocity) measurement noise, e.g., 1% noise can cause over 5% identification error.

   – The identification process is much less sensitive to measurement errors when the initial angular momentum is known (i.e., option 1 of the method) than unknown (i.e., option 2 of the method).

6) When using solar arrays for inertia identification,

   – The solar arrays must be motion controllable.

   – If the satellite initially rotates about only one axis, then the solar arrays have to be able to rotate in two axes in order to identify all the inertia matrix.

49

- The method is insensitive to sensor noise for identifying mass and mass-center location. But it is sensitive to sensor noise for identifying the inertia tensor.

- Other findings of the method should be similar to these by using a robotic arm.

Recommendation for further study:

1) Complete the study of using a solar-array mechanism
2) Continue the research to address the issue of sensitivity to sensor noise
3) Investigate the concern about external disturbances
4) Design an air-bearing based testbed for experimental verification
5) Explore ideas of using other means, e.g., known fuel level

6. REFERENCES

[1] T. Kasai, M. Oda and T. Suzuki, "Results of the ETS-7 mission – rendezvous docking and space robotics experiment", Proc. 5th Int. Symp. on Artificial Intelligence, Robotics and Auto. in Space, Nordwijk, The Netherlands, pp.299-306., 1999.

[2] D.P. Seth, "Orbital Express: Leading the way to a new space architecture", 2002 Space Core Tech Conference, November 19-21, 2002, Colorado Springs.

[3] Bosse A.B. et al., "SUMO: Spacecraft for universal modification of orbits", *SPIE Defence and Security Symp.*, Orlando, FL, Apr 2004, Proc. SPIE Vol.5419, pp.36-46.

[4] G. Hirzinger et. al., "DLR's robotics technologies for on-orbit servicing", Advanced Robotics, Vol.18, No.2, 2004, pp.139-174.

[5] E. Dupris, M. Doyon, E. Martin, P. Allard, J.C. Piedboeuf, and O. Ma, "Autonomous Operations for Space Robots", Proc., 55th International Astronautical Congress, Vancouver, Oct.4-8, 2004, Paper #IAC-04-IAA.U.5.03.

[6] B. Liang, C. Li, L. Xue, and W. Qiang, "A Chinese small intelligent space robotic system for on-orbit servicing", Proc. IEEE Int. Conf. on Intelligent Robots and Systems, Beijing, China, Oct.9-15, pp.4602-4607.

[7] E.V Bergmann, B.K. Walker, and D.R. Levy, "Mass property estimation for control of asymmetrical satellites", J. of Guidance, Control, and Dynamics, Vol.10, No.5, 1987, pp.483-491.

[8] R.F. Richfield, B.K. Walker and E.V. Bergmann, "Input selection and convergence testing for a second order mass property estimator," Journal of Guidance, Control, and Dynamics, Vol. 11, 1988, pp. 207-212.

[9] E.V. Bergmann and J. Dzielski, "Spacecraft mass property identification with torque-generating control," Journal of Guidance, Control, and Dynamics, Vol. 13, 1990, pp. 99-103.

[10] J. Palimaka, and B.V. Burlton, "Estimation of spacecraft mass properties using angular rate gyro data," AIAA/AAS Astrodynamics Conf., Hilton Head Island, SC, Aug. 10-12, 1992, pp. 21-26.

[11] S. Tanygin and T. Williams, "Mass property estimation using coasting maneuvering", J of Guidance, Control, and Dynamics, Vol.20, No.4, 1997, pp.625-632.

[12] E. Wilson, C. Lages, R. Mah, "On-line, gyro-based, mass-property identification for thruster-controlled spacecraft using recursive least squares", Proc. of 45th IEEE Midwest Symp. on Circuits and Systems, Tulsa, OK, pp.334-337, Aug.4-7, 2002.

[13] M.A. Peck, "Mass-properties estimation for spacecraft with powerful damping", Proc. AAS/AIAA Astrodynamics Specialist Conf., Girdwood, Alaska, Aug.16-19, 1999.

[14] Y. Murotsu, K. Senda, M. Ozaki, and S. Tsujio, "Parameter identification of unknown object handled by free-flying space robot", J. of Guidance, Control and Dynamics, Vol.17, No.3, 1994, pp.488-494.

[15] K. Yoshida and S. Abiko, "Inertia Parameter Identification for a Free-Flying Space Robot," *Proc. of AIAA Guidance, Navigation, and Control Conf.*, AIAA 2002-4568, Monterey, CA, August 2002.

[16] Ma and S. Horan, "NMSU Nanosatellite with robotics capabilities", Proc. of 8th International symp. on Artificial Intelligence, Robotics and Automation in Space, Munich, Germany, Sept.5-9, 2005, pp.145-148.